SANDIA REPORT
SAND2008-6978
Unlimited Release
Printed October 2008

Fabrication of Large-Volume, Low-Cost Ceramic Lanthanum Halide Scintillators for Gamma Ray Detection

Final Report for DHS/DNDO/TRDD Project TA-01-SL01

Pin Yan, Timothy J. Boyle, Nelson S. Bell, Margaret R. Sanchez, Leigh Anna M. Ottley, and Ching-Fong (Chris) Chen

Prepared by
Sandia National Laboratories
Albuquerque, New Mexico 87185 and Livermore, California 94550

Sandia is a multiprogram laboratory operated by Sandia Corporation,
a Lockheed Martin Company, for the United States Department of Energy's
National Nuclear Security Administration under Contract DE-AC04-94AL85000.

Issued by Sandia National Laboratories, operated for the United States Department of Energy by Sandia Corporation.

Available to DOE and DOE contractors from
U.S. Department of Energy
Office of Scientific and Technical Information
P.O. Box 62
Oak Ridge, TN 37831

Telephone: (865) 576-8401
Facsimile: (865) 576-5728
E-Mail: reports@adonis.osti.gov
Online ordering: http://www.osti.gov/bridge

Available to the public from
U.S. Department of Commerce
National Technical Information Service
5285 Port Royal Rd.
Springfield, VA 22161

Telephone: (800) 553-6847
Facsimile: (703) 605-6900
E-Mail: orders@ntis.fedworld.gov
Online order: http://www.ntis.gov/help/ordermethods.asp?loc=7-4-0#online

SAND2008-6978
Unlimited Release
Printed (October/2008)

Fabrication of Large-Volume, Low-Cost Ceramic Lanthanum Halide Scintillators for Gamma Ray Detection

Pin Yang, Timothy J. Boyle, Nelson S. Bell, Margaret R. Sanchez and
Leigh Anna M. Ottley
Sandia National Laboratories

Ching-Fong (Chris), Chen
Los Alamos National Laboratory

Sandia National Laboratories
P.O. Box 969
Livermore, CA 94551

ABSTRACT

This project uses advanced ceramic processes to fabricate large, optical-quality, polycrystalline lanthanum halide scintillators to replace small single crystals produced by the conventional Bridgman growth method. The new approach not only removes the size constraint imposed by the growth method, but also offers the potential advantages of both reducing manufacturing cost and increasing production rate. The project goal is to fabricate dense lanthanum halide ceramics with a preferred crystal orientation by applying texture engineering and solid-state conversion to reduce the thermal mechanical stress in the ceramic and minimize scintillation light scattering at grain boundaries. Ultimately, this method could deliver the sought-after high sensitivity and <3% energy resolution at 662 keV of lanthanum halide scintillators and unleash their full potential for advanced gamma ray detection, enabling rapid identification of radioactive materials in a variety of practical applications.

This report documents processing details from powder synthesis, seed particle growth, to final densification and texture development of cerium doped lanthanum bromide ($LaBr_3:Ce^{+3}$) ceramics. This investigation demonstrated that:

- A rapid, flexible, cost efficient synthesis method of anhydrous lanthanum halides and their solid solutions was developed. Several batches of ultrafine $LaBr_3$:Ce^{+3} powder, free of oxyhalide, were produced by a rigorously controlled process.
- Micron size (~ 5 μm), platelet shape $LaBr_3$ seed particles of high purity can be synthesized by a vapor phase transport process.
- High aspect-ratio seed particles can be effectively aligned in the shear direction in the ceramic matrix, using a rotational shear-forming process.
- Small size, highly translucent LaB_3 (0.25" diameter, 0.08" thick) samples were successfully fabricated by the equal channel angular consolidation process.
- Large size, high density, translucent $LaBr_3$ ceramics samples (3" diameter, > 1/8" thick) were fabricated by hot pressing, demonstrating the superior manufacturability of the ceramic approach over single crystal growth methods in terms of size capability and cost.

Despite all these advances, evidence has shown that $LaBr_3$ is thermally unstable at temperatures required for the densification process. This is particularly true for material near the surface where lattice defects and color centers can be created as bromine becomes volatile at high temperatures. Consequently, after densification these samples made using chemically prepared ultrafine powders turned black. An additional thermal treatment in a flowing bromine condition proved able to reduce the darkness of the surface layer for these densified samples. These observations demonstrated that although finer ceramic powders are desirable for densification due to a stronger driving force from their large surface areas, the same desirable factor can lead to lattice defects and color centers when these powders are densified at higher temperatures where material near the surface becomes thermally unstable.

ACKNOWLEDGMENTS

This work was performed under the auspices of the U.S. Department of Energy as work for others funded by the U.S. Department of Homeland Security, Domestic Nuclear Detection Office, Transformational Research and Development Directorate.

The authors would like to acknowledge Christina M. Baros, Robin M. Sewell, Mark A. Rodriguez, Harry D. Pratt, Clay S. Newton, Christopher B. DiAntonio, Bonnie McKenzie, and Richard P. Grant for their technical support. Technical guidance and program support from William P. Ballard, Paul D. Rocket, F. Patrick Doty, James P. Wilhelm, James C. Lund, Mark N. Allen, and David M. Weaver are also greatly appreciated.

Figures

Tables

OVERVIEW

Improved scintillators are critical to the Domestic Nuclear Detection Office's (DNDO's) mission of advancing the technology for detecting and identifying special nuclear material (SNM) and other radiological materials. Literature has shown that cerium doped lanthanum halides, such as $LaCl_3$:Ce and $LaBr_3$:Ce, have exceptional scintillation properties at room temperature for gamma ray detection, (see Figure 1).[1]

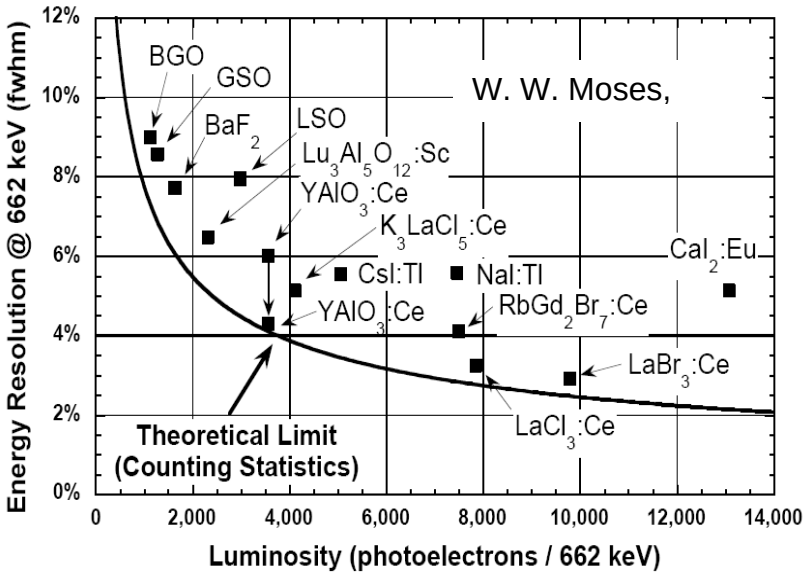

Figure 1. Measured energy resolution of several scintillators as a function of their light output

These materials possess sufficient stopping power for detection, as well as excellent luminosity, high spectral energy resolution at room temperature, short decay time, and significant proportional output.[2] Lanthanum halide scintillators reported to date have been produced mainly by the conventional Bridgman growth method in small diameter quartz tubes. During the transition from a laboratory curiosity to a practical application, several manufacturability issues have surfaced. For example, because large lanthanum bromide single crystals are mechanically fragile and temperature sensitive, they are difficult to grow in large sizes due to process-induced cracking from cleavage planes uniquely associated with low strength and low toughness single crystal materials. These issues lead to a low production yield and a high manufacturing cost, and have hampered progress towards manufacturing practical volume detectors.

This project focuses on replacing the conventional Bridgman (single crystal) growth method with advanced ceramic processes to fabricate optical quality lanthanum halide scintillators. The advanced approach provides significant advantages. Foremost, because polycrystalline ceramics in general are much stronger and tougher than single crystal materials, the ceramic approach will

---

[1] E. V. D. Van Loef, P. Dorehbos, and C. W. E. Van Ejik, K. Kramer, and H.U. Gudel, *Applied Physics Letters*, **79** [10] 1573 (2001), and *Nuclear Instruments & Methods in Physics Research*, **A486** 254 (2002).

[2] William W. Mosses, *Nuclear Instruments & Methods in Physics Research*, **A487** 123 (2002).

increase material and device fabrication yields by reducing machining and handling losses—thereby reducing manufacturing costs and enhancing the production rate. Furthermore, the new approach is able to produce larger crystals, overcoming the size limitations encountered with the Bridgman method.

The ultimate goal of this project is to use a cost-effective advanced ceramic processing approach to deliver lanthanum halide scintillators with the sought-after high sensitivity and <3% energy resolution at 662 keV.[1] Reaching this goal would unleash the full potential of these scintillators for advanced gamma ray detection, enabling rapid identification of radioactive materials in a variety of practical applications.

With these objectives, this work focused on developing $LaBr_3:Ce^{+3}$ ceramics which can meet the aforementioned performance metrics. Special emphasis was placed on powder synthesis and advanced ceramic processing approaches that enable the manufacturing of optical quality ceramics. Optical quality ceramics require high purity and high density to minimize light absorption and light scattering in the material. To achieve high purity and high density ceramics, the starting powder needs to have a large surface area to enhance the densification, as well as developing a synthesis route that can produce high purity and chemically homogeneous powder. In addition, rigorous process control and handling is required due to the hygroscopic nature of the lanthanide halides to prevent any foreign phase formation which in turn will enhance the light scattering in the material. Furthermore, $LaBr_3$ is a strongly birefringent material - with refractive indices of 1.90 and 1.95 in the different optical axes. This can lead to significant light scattering at grain boundaries due to refractive index mismatches as a result of the randomness of crystal orientations in a polycrystalline ceramic. This issue was addressed by producing a textured ceramic where crystallographic orientations of individual grains are highly aligned; significantly reducing refractive index mismatches at the grain boundary. To create such a microstructure, high aspect ratio, micron-size seed crystals are needed to define a preferred crystal orientation in a ceramic powder matrix through a localized shearing process, followed by a solid state conversion[3,4] and densification. During densification, these aligned seed crystals, acting as templates, grow in the expanse of the ceramic matrix and eventually form a dense ceramic. This process is important to achieving a fully textured ceramic body with significantly reduced light scattering at the grain boundary. Therefore, this program is composed of three subtasks, including (1) synthesis of ultra-fine, high purity $LaBr_3:Ce^{+3}$ powder, (2) growth of high aspect ratio $LaBr_3$ seed crystals, and (3) densification and texture development. A mitigation plan, using a novel equal channel angular consolidation was also explored.

[3] T. Yamamoto and T. Sakuma, *J. Am. Ceram. Soc.*, **77** [4] 1107 (1994).

[4] C. Scott, J. Strok, and L. Levison, U.S. Pat. No. 5 549 746 (1996).

2. TECHNICAL PROGRESS ACHIEVED AGAINST GOALS

In a previous report[5], we developed a low-cost, flexible synthesis route to fabricate lanthanide halide hydrates. These hydrates were then converted to anhydrous powder through vacuum dehydration. Furthermore, evidence showed that at temperatures below 200°C, lanthanide halides and their Ce^{+3} activator for scintillation readily formed a complete solid solution. However, details in the dehydration process, structure evaluation from crystalline hydrates to anhydrous powder, and phase relationship with $CeBr_3$ were not studied. Large size, highly anisotropic seed crystals were fabricated from a hot solution were thermally stabilized and incorporated in the ceramic matrix by a rotational shear forming process. After densification, these crystals were found to be aligned in the shear direction and dense, pore-free regions were observed near the seeds. However, the nature of these seed particles after the thermal process was not clear and the seed-ceramic interface needed further characterization. Lastly, we have demonstrated the ceramic approach is more manufacturable than the single crystal growth method in terms of size capability, cost, and yield, by fabricating two large translucent samples (3" diameter, > 1/8" thick) though hot pressing. In this report, we documented details of these unreported issues and achievements for the challenges that arose during this development program.

Three major tasks were established in the Phase II and Phase III programs to achieve the project goals, which include:

- Synthesis of ultrafine, high purity $LaBr_3$-$CeBr_3$ ceramic powders which enable effective densification for ceramic scintillators to achieve optical quality. Major milestones and deliverables include (1) demonstrate the scale up capability for powder synthesis for batches greater than 100 grams, (2) identify and eliminate the sources of processing inconsistency, (3) eliminate all contaminants and prevent oxyhalide formation, (4) obtain a basic understanding and experimental evidence of the cause of the darkening of $LaBr_3$ after high temperature densification, and (5) develop a water-free synthesis route for $LaBr_3$.
- Preparation of seed particles with proper morphology and size, which are keys to developing a crystallographically oriented (or "textured") ceramic. Major tasks include (1) characterize the thermally stabilized seed crystals synthesized from tetrahydrofuran (THF) by a hot solution method, and (2) develop an alternative synthesis route (gas transport process) for the seed crystal synthesis. Due to time, Environment, Safety and Health (ES&H) considerations, and resource constraints, this activity ended after the Phase II development had finished.
- Development of dense, textured ceramics. Densification and texture development will help to remove residual porosity and to minimize light scattering in polycrystalline ceramics. Major tasks include (1) continue evaluating the rotational shear forming process, (2) develop an alternative process to promote densification and texture development, (3) develop a carbon and oxygen free hot pressing capability for densification, and (4) explore equal channel angular consolidation process.

---

[5] P. Yang, T. J. Boyle, and N. S. Bell, "Fabrication of large-volume, low-cost ceramic lanthanum halide scintillators for gamma ray detection – Annual Report for Phase 1 of DHS/DNDO/TRDD project TA-01-SL01," Sandia Report, SAND2007-0719, Sandia National Laboratories, Albuquerque, New Mexico 87185, (2007).

We have met the majority of our objectives and milestones for these tasks. However, due to unforeseen challenges in the development stage we were unable to explore the solid-state conversion process for texture development, to improve the optical quality of ceramic by processing-microstructure-property relationship, and evaluate the scintillation properties of densified ceramics.

Anhydrous $LaBr_3:Ce^{+3}$ powder were obtained by vacuum dehydration of hydrates synthesized by a direct acidification process. In addition, we have constructed a binary phase diagram between $LaBr_3$ and $CeBr_3$, based on x-ray structure refinement and thermal analysis data. Details of the vacuum dehydration of $LaBr_3 \cdot 7H_2O$ as well as the structural phase evolution of different hydrates were investigated. The dehydration involves several reconstructive phase changes as bound water is progressively removed from the hydrate. Results have shown that vacuum plays an important role in lowering the dehydration temperature. However, the poor heat transfer though a thick powder during vacuum dehydration (i.e., no convectional heat flow) can be problematic and creates inconsistencies in removing all the residual water. It is found that employing either a fluidized reactor or an additional bromine gas treatment can significantly minimize the processing variations. Furthermore, handling these extremely hygroscopic materials in all processes has deemed to be crucial to prevent oxyhalide (LaOBr) phase formation. A large quantity of phase pure $LaBr_3:Ce^{+3}$ powder (> 80 grams) were synthesized with the help of these process improvements. This powder was demonstrated to be anhydrous (< 100 ppm water in the powder) by multinuclear NMR studies.

The challenges in the dehydration process prompted us to investigate an alternative approach to removing water from the lanthanum bromine hydrates, using substitution of water by other Lewis bases such as methanol (MeOH). A number of analytical processes monitored the de-solvation process. Results demonstrated that the de-solvated $LaBr_3(MeOH)_4$ can be successfully converted to anhydrous $LaBr_3$.

High aspect–ratio seed crystals have been successfully prepared by a hot solution method, using tetrahydrofuran (THF). These seeds luminance under electron beam stimulation (or cathodoluminescence). Thermal analysis and Transmission electron microscopy (TEM) were used to characterize these seed particles. TEM results have shown that there large seed crystals turned into nanocrystalline aggregates after being thermally stabilized at high temperature (see previous report[5]). The observation is consistent with the thermal analysis results where multiple thermal events and weight losses were involved during the heating cycle, suggesting these seeds might have gone through several structure phase transformations - a similar process to the dehydration of lanthanum bromine hydrates. As a result, they lost their function as templates for texture development later in the densification process. Details of the structure phase transformations were not studied, as it was not the major focus of this investigation.

Preparation of seed crystals from solution was soon abandoned as it was found to be high risk because of the complexity of understanding the structure phase transformations involved with the removal of bound water or organics (such as methanol, ammonia, and THF) from the precursor material (such as hydrates and $La(MeOH)_5$). An alternative approach, using a gas phase transport method, was developed based on literature. The process has shown some success in producing micron size, hexagonal shaped $LaBr_3$ platelet seed crystals. However, the use of highly corrosive

bromine gas as well as the ES&H issues associated with scaling up of this process has limited our effort in pursuing this approach.

Our previous work has shown that after densification samples prepared by the dehydration process turned black. The darkening observed at that time was attributed to possible carbon contamination due to the using a graphite resistive heating element. Therefore, during the last phase of development, we established a high pressure hot pressing system (10 kpsi Inconel die in comparison to 5 kpsi with a graphite die) with a RGA gas monitoring system in an argon filled glovebox. Samples after hot pressing showed a strong a-axis out-of-plane texture (based on hexagonal setting) and a significant grain growth. Fully densified ceramics with grain size as large as 20 mm x 4 mm was observed. It was also found that the extent of grain growth and texture development is quite sensitive to the applied pressure. This result suggests that highly textured ceramics can be made without introducing template seed particles. The combined effects are highly desirable since textured ceramics can reduce refractive index mismatch at grain boundaries, and the abnormal grain growth can replace the solid-state conversion process to create a large grain microstructure. These results will improve the ceramic transparency by reducing the amount of light scattering at the grain boundary.

Severe plastic deformation such as equal channel angular extrusion has been commonly used in metal systems to create a new class of material with ultrafine grain microstructure (< 300 nm). Because of the low melting point of $LaBr_3$, Sandia has collaborated with Los Alamos National Laboratory to develop a equal channel angular consolidation (ECAC) process for densification of nanocrystalline $LaBr_3$:Ce^{+3} powder prepared by melt-spin process, as a part of our risk mitigation contingency plan. The process was the first of its kind and involved a consolidation process with a concurrent deformation in forming and densification processes to achieve high density and ultrafine grain microstructure, and was nominated for R&D100 award from Los Alamos National Laboratory. The nanocrystalline $LaBr_3$:Ce^{+3} powder was sealed in a nickel can and processed at 720°C at 15 kpsi with single pass. Dense samples (0.25” diameter, 0.08” thick) after consolidation appeared to be highly translucent. The process demonstrates a feasible way to improve the transparency in nanostructured $LaBr_3$ ceramics for scintillator applications. Because of the size limitations with the current ECAC step-up at Los Alamos and budget constraints, this approach was no longer pursued at the end of the second phase of development.

The darkening of chemically prepared $LaBr_3$ powder after the high temperature densification process was observed from the first phase of development. This behavior could be attributed to (1) carbon contamination, (2) reduction of the lanthanum bromide phases, (3) foreign phase formation, or (4) intrinsic thermal stability near the surface layer of these compounds. To identify which mechanism controls the darkening behavior is quite challenging since most analytical methods that have been explored, including X-ray diffraction, electron microprobe analysis, electron spin resonance measurements, and induction coupled plasma atomic emission spectroscopy, all have their own limitations on giving a quantitative analysis on the structural defects developed in the $LaBr_3$ during high temperature processing. Therefore, a systematic deductive reasoning approach was used to study the root-cause of the darkening behavior. It was found that $LaBr_3$ was thermally unstable at temperatures required for densification process (> 450°C). This is particularly true for material near to the surface where lattice defects and color centers can be created as bromine becomes volatile at high temperatures. Consequently, after

densification these samples made by chemically prepared ultrafine powders turned black. An additional thermal treatment in a flowing bromine condition has proven to be able to reduce the darkness of the surface layer for these darkened samples. The intrinsic stability of these lanthanide halide compounds gives an ultimate challenge in fabrication of optical quality, ceramic scintillators from a chemically prepared, ultra-fine powder.
Table 1 summarizes our accomplishments against goals and the following subsections discuss progress in detail.

Table 1. Project tasks and accomplishments

Tasks		Progress/ Accomplishments	Last Report Status	Current Report Status
1.1	Large batch synthesis/dehydration	Non-static vacuum and bromine assisted dehydration process have improved the dehydration process, but still cannot completely eliminate the LaBrO formation. The use of a fluidized reactor further improved the efficiency. Process control seems to be the key to achieving anhydrous powder.	One week behind	Continue with Task 3.1
1.2	Controlled recrystallization	Seeding procedure has been introduced during dehydration process. Freeze drying has been explored. SEM results show that neither approach produces desirable template seed particles.	Task terminated	N/A
1.3	$LnX_3\,nH_2O$ synthesis	Evaluation is near completion. (Supported by a Sandia internal resource)	Task terminated	N/A
1.4	Vapor phase synthesis of template seed crystals	LaBr3 crystals confirmed by XRD using vapor route, but morphology control still needs to be established. Silicon contamination was found in a closed quartz reactor. A new alumina reactor will be used to minimize the contamination. Synthesis conditions are being evaluated.	Two weeks behind	On Hold
1.5	Solution solubility measurements	Solvent testing of solubility is no longer required. Action item is terminated.	Task terminated	N/A
1.6	Hot solution route	Action terminated by choice of 1.4	Task terminated	N/A
1.7	Seed particle characterization	Thermal treated seed particles exhibit polycrystalline nature. New approaches include vapor phase deposition and controlled recrystallization will be investigated	N/A	N/A
1.8	Water removal	Activity has focused on generating water free species through the substitution of methanol and the presence of a drying agent (MeOH).	In Progress	Task completed

Tasks		Progress/ Accomplishments	Last Report Status	Current Report Status
1.9	Synthesis of template crystals – evaporation route	Needle shape crystals were isolated from anhydrous MeOH, and the crystal structure was determined. Solution routes found to maintain organic content, so this route is not being pursued further.	Task terminated	N/A
1.10	Pressure induced abnormal grain growth and texture development	A new approach to fabricate highly textured ceramics with millimeter size grains has been developed. Results were confirmed and a partially translucent sample was fabricated. The repair of hot press done. New experiments have been planned.	New	Two weeks behind
1.11	Equal channel angular sintering	The ECAC process has fabricated three samples. A translucent sample was made by single pass. Process improvement to enhance the optical quality is underway.	On Schedule	Task terminated
1.12	Verify residual water by NMR study	Results from NMR studies of label 17O and solid state 139La indicate that our vacuum evaporation is effective to remove residual water for initial lanthanum bromide hydrates.	New	Task completed
2.13	Control oxygen contamination	Powders prepared under different conditions were sealed in quartz tubes and fired at 700°C, to verify the oxybromide formation. A new Schlenk system for bromine treatment has been designed and sent to fabrication.	On schedule	Task terminated
2.1	Optimize dopant level	Based on quarterly review decision, all effort will focus on La0.95Ce0.05Br3.	One week behind	on hold
3.0	Finalize Statement of work for Phase III	Revision was made based on program manager's feedback	N/A	Task completed
3.1	Control oxygen during synthesis and handling	A large batch of LaBr3 powder was made from the new Schlenk system. Procedures to avoid leakage from end caps were identified. New batch of cerium doped lanthanum bromide powders were synthesized to support experimental work.	On schedule	Task completed
3.2	Set up in-house hot-press and gas monitoring system	The new glovebox was equipped with a RGA system. The RGA system was tested and evaluated. Components for hot press were purchased. An out gassing procedure for the refractory was performed both in air and in argon glove box. Hot pressing experiments were performed successfully with the new capability. Samples remain dark. However, the dark appearance seems to correlate to the processing time.	On schedule	Task completed
3.3	Melt experiments in sealed quartz ampoules	Melt experiments were performed. Results demonstrated the importance of process environment and powder handling. Results	On schedule	Task completed

Tasks		Progress/ Accomplishments	Last Report Status	Current Report Status
		suggest that darkening might be induced by thermal process		
3.4	Thermal stability study	Comparing the weight loss between coarse commercial powder and chemically synthesized powder – a deductive reasoning approach	New	Task completed

Status color code definitions: R= Task completion at risk, Y= Milestones/Deliverables at risk, G=Task proceeding as planned, B=Task completed

2.1 Progress Details

2.1.1 Task 1: Chemical synthesis of lanthanum halides

2.1.1.1 Development Approach

High purity, oxyhalide-free powder is an essential starting material, since even trace impurities can significantly degrade scintillation performance. In addition, obtaining optical quality ceramics requires the powder provided for the final densification process to achieve high sintering activity, which demands a finer powder, preferably of submicron size, to promote densification. In the presence of seed particles, a fine powder matrix can nurture the seed particle growth that is important for texture development. Further, solution synthesis provides an unparalleled advantage when the activator (Ce^{+3}) must be homogeneously distributed into the solid solution to ensure uniform scintillation across the detector. Because many of these characteristics cannot be found in commercial powders, a task was identified to address these issues. In the process development, we evaluated many synthesis routes, both from literature and from our original work, with emphasis on the cost of precursors, process efficiency, simplicity, and scale-up capability, since these elements are key to addressing manufacturability and cost issues. Other considerations include activator incorporation, size, and morphology control. A special preference will be given to a process that can avoid water due to the hygroscopic nature (i.e., extreme sensitivity to moisture) of lanthanum halides.

2.1.1.2 Development Details

(1) Direct Acidification for lanthanum halide hydrates synthesis

We have successfully generated LnX_3 (Ln = La and Ce; and X = Cl, Br, I) from the reaction of Ln^o and the appropriate HX by a direct acidification process developed in Sandia (Sandia Technical Advance: SD-10592/S-111186).

$$Ln^o + (xs)HX \xrightarrow{neat} \{[Ln(\mu - X)(H_2O)_7][X]_2\}_2 \qquad (1)$$

The resulting products have been identified by single crystal XRD as $[(H_2O)_7Ln(\mu\text{-}X)][X]_2$. This simple approach has demonstrated to be flexible in synthesizing all the lanthanide halide

hydrates as well as hydrates for the IIIB elements (such as yttrium and scandium). These hydrates yield three general structure type; (1) dimmer with two inner sphere (IS) halides (terminal and bridging) and one outer sphere (OS) anion, (2) mononuclear 2IS/1OS with variable salvation, and (3) mononuclear 3 OS anions. Each dinuclear species was found to adopt a 9-coordinated arrangement where each monomer varies in geometry from 9 to 8 to 7 based on the number of bounded water present, as they are shown in Figure 2 (using the lanthanide bromides as examples). Details about the structural refinements are reported elsewhere.[6]

The hydrated lanthanum and cerium bromides, $La_{1-x}Ce_xBr_3$ nH_2O, were prepared from the direct acidification process shown in Equation 1. The appropriate lanthanide metal (Ln^o) was weighed out from either a chip of the stock metal or as a powder in the desired stoichiometry prior to dissolution in excess hydrobromic acid in an argon filled, dry glove box. After the initial effervescence was complete and the metal completely consumed, the clear solution was transferred into a Schlenk flask, placed in a hot water bath, and the volatile component removed by vacuum distillation to dryness. A small amount of the as-dried powder was characterized by simultaneous thermal gravitational (TGA) and scanning thermal calorimetry (DSC) measurements (NETSCH STA449C) to determine its dehydration behavior, and both melting and freezing points. The rest of the powder was subsequently dehydrated in a hot oil bath (~180 °C) under vacuum (10^{-3} torr) for several hours. The dry powder was transferred to the glove box and was ground in an alumina mortar and pestle, and forced through a 125 μm nylon mesh sieve. The ground powder was dried again on the hot oil bath under vacuum for additional 4 - 6 hours to remove residual water. The resulting anhydrous powder was then used for all subsequent X-ray diffraction analyses.

(2) Dehydration under vacuum

The dehydration behavior of the $La_{1-x}Ce_xBr_3$ nH_2O powder was studied under vacuum conditions in the STA to be consistent with the drying procedure used for powder preparation. Approximately 20 mg of the $La_{1-x}Ce_xBr_3$ nH_2O powder was placed in an alumina crucible covered with a lid. Previous results indicated alumina would not react with lanthanide bromide up to its melting point.[5] The powder was heated from room temperature to 200°C under vacuum at 1 °C/min and held at 200°C for 20 minutes. Thermal events and weight loss were recorded during the dehydration process. After the holding period, the vacuum was turned off and the atmosphere switched to flowing argon (at 50 ml/min.). Different heating rates, ranged from 0.25°C/min to 5°C/min were also collected for few specific compositions to compare the kinetics of the dehydration process. These results were compared with the dehydration behavior of single crystal lanthanum bromide heptahydrate. Unless it is specifically pointed out, data are reported at 1°C/min. The resulted powder was subsequently heated to 810 °C at 3 °C/min. The sample was held for 5 minutes, and then cooled back to room temperature at 3°C/min. During this thermal incursion, both melting point and freezing point for the $La_{1-x}Ce_xBr_3$ solid solution were

---

[6] T. J Boyle, L.A. M. Ottley, M. A. Rodriguez, T. M. Alam, P. Yang, S. Hoppe, R. M. Sewell, C. M. Baros, S. K. McIntyre, M. R. Sanchez, "Facile synthesis of structurally characterized lanthanide/group 3 halide hydrates, anhydrous halides and solid solution of mixed lanthanide halide materials," submitted to *Inorganic Chemistry*, 92008).

determined at the peak temperature of the endothermic and the exothermic events from the DSC measurements.

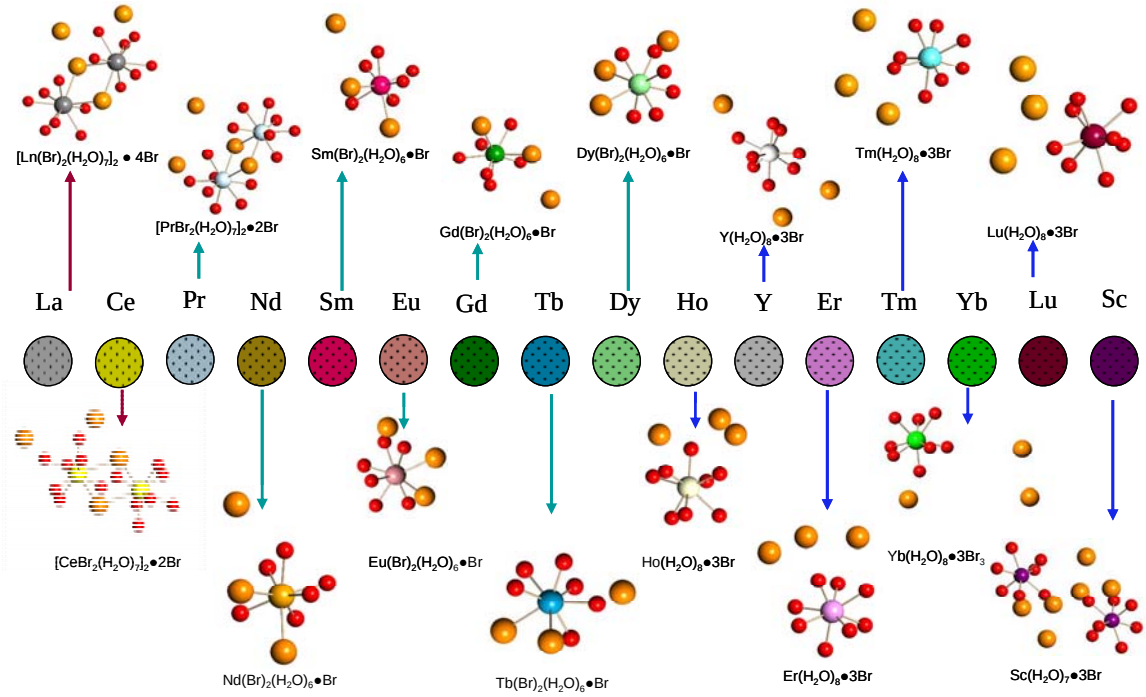

Figure 2. Different hydrate structures synthesized by the direct acidification process.

$La_{1-x}Ce_xBr_3$ powders were prepared for X-ray diffraction (XRD) analysis using a specially designed holder for air/moisture sensitive materials. The holder employed a "Beryllium Dome" (BeD) to allow access of the X-ray beam to the specimen.[15] For rigorous exclusion of air and moisture, the specimen was prepared inside a glove box. Powder was placed on a zero-background slide (1cm dia.), loaded into the BeD holder, and sealed via a compression O-ring so as to preserve the atmospheric conditions of the glove box. The holder was removed from the glove box and directly transported to the Siemens D500 XRD unit for analysis. The XRD unit employed a sealed-tube Cu anode X-ray source (40 kV, 30 mA), a diffracted-beam graphite monochromator, and fixed (1^o) slits. Typical scan conditions were 5-80^o 2θ, 0.04^o 2θ step-size, and 1 sec count-time. Scan conditions used for structural analysis were 20-120^o 2θ, 0.04^o 2θ step-size, and 20 sec count-time. Results of the thermal analysis and X-ray diffraction measurements were confirmed with four replicated compositions of the $La_{1-x}Ce_xBr_3$ solid solution.

To understand the structural phase evolution and to refine weight loss during the dehydration process, single crystals of $LaBr_3$ heptahydrate were prepared. These single crystals were recrystallized from a hot, oversaturated hydrobromic acid solution prepared by the direction acidification process. These crystals were isolated and dried in the argon glovebox for detailed thermal analysis and high temperature X-ray study. Single crystals were first crushed for the

structural refinement by the Be-D XRD study.[7] Results confirm that these crystals are $LaBr_3$ heptahydrate. High Temperature X-ray Diffraction (HTXRD) was performed, using a Scintag PAD X1 diffractometer equipped with a sealed-tube Cu X-ray source, an incident beam X-ray mirror optic, and a Peltier-cooled solid-state Ge detector, to study the structural evolution during dehydration process. Generator settings of 40kV and 30mA were used for generation of Cu Kα radiation from the X-ray anode. Incident and diffracted beam scatter slits (1 mm) were employed for beam columniation. The diffractometer was equipped with a Bühler HTK 1.4 hot stage. The heating chamber was equipped with a gas handling system for flowing inert gas (He). An oxygen getter was plumbed in the gas stream prior to the hot-stage chamber. An oxygen detector was configured at the downstream portion of the gas-flow plumbing to monitor oxygen partial pressure within the chamber during heat treatment cycling of the sample. The gettered He gas showed < 0.1 ppm O_2 presence for the entire heating cycle. The sample was heated in 5 °C increments from 30 °C to 120 °C with a heating rate of 5°C/min between temperature steps. At each hold temperature, θ–2θ scans were collected over the range of 5-60 °2θ with a step-size of 0.05° and count time of 0.5 sec. A total of 6 scans (~12 min/scan) were collected at each temperature for a total of ~72 minutes hold-time at each temperature increment.

The general behavior of thermal dehydration, characterized by the thermal analysis, for all compositions of the $La_{1-x}Ce_xBr_3$ solid solution systems is quite similar. Figure 3 shows the dehydration of hydrate crystals isolated directly from a supersaturated HBr solution under vacuum with a heating rate of 0.25°C/min., results show a weight loss amounts to 24.20 wt%, which is consistent with loss of all the bound waters associated with lanthanum bromide heptahydrate (theoretical value of 24.99%).

The DSC (dotted line in Fig. 3) and TGA (solid line) measurements detected three major endothermic events (at 36.5 °C, 64.7 °C, and 112.1 °C), which indicates that several intermediate hydrates are formed during dehydration. Weight change from heptahydrate to anhydrous $LaBr_3$ is labeled on the right in Fig. 1. Based on weight loss measurements, horizontal weight levels between the second and the third endothermic events (3.47% compared to the theoretical value of 4.54%), and the first and the third endothermic events (10.27%, compared to the theoretical value of 12.49%) correspond to the formation of a monohydrate and a trihydrate ($LnBr_3$ $3H_2O$), respectively. These measured peak temperature and the amount of weight loss associated with each endothermic event increase with increasing heating rate. Additional small endothermic events have often been observed at fast heating rates (i.e., 1°C/min. and 5°C/min., and are similar to results reported for dehydration in flowing nitrogen.[8] These small endothermic peaks occur between the three major endothermic events and may be either distinct from or overlap the major events. However, the weight loss during these small events is almost continuous; suggesting the kinetics of dehydration is dominant since the activation energy for these dehydration steps is

[7] M. A. Rodriguez, D. Harris, T. J. Boyle and P. Yang, "A Beryllium Dome Specimen Holder for XRD Analysis of Air Sensitive Materials," *Powder Diffraction*, **23** [2], 121-4, (2008)

[8] S. J. Ashcroft and C. T. Mortimer, "The thermal decomposition of lanthanide (III) chloride hydrates," *J. Less-Common Metals* 14, 403-406 (1968).

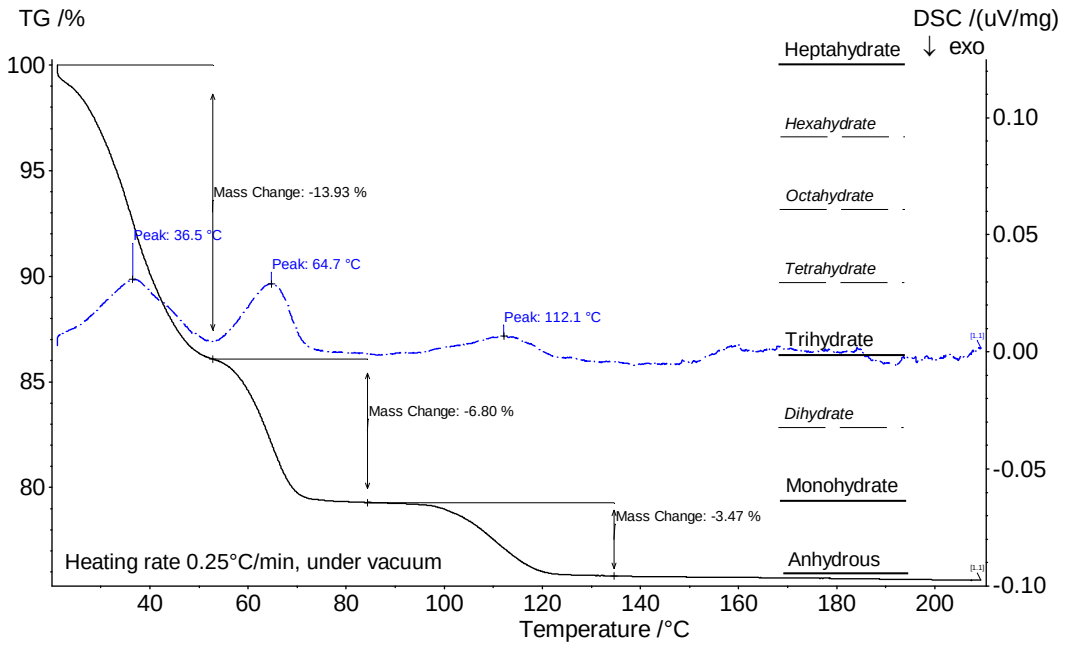

Figure 3. The thermal dehydration behavior of $LaBr_3 7H_2O$ single crystals in vacuum. The solid line represents the thermal gravitational analysis and the dotted line shows the thermal calorimetry measurement.

small. This argument seems to be supported by the evidence that when a faster heating rate[9, 10, 11] (> 5°C/min) is used during dehydration, only one horizontal level of weight loss is detected, which corresponds to a continue but overlapped decomposition of intermediate hydrates from heptahydrates to anhydrous lanthanum halides. These observations highlight the importance of the kinetic factors (i.e., heating rate and vacuum) in characterization of the dehydration process.

The vacuum dehydration (10^{-3} Torr) temperatures for the decomposition of major hydrates, such as $LnBr_3 7H_2O$, $LnBr_3 3H_2O$ and $LnBr_3 H_2O$, in the $La_{1-x}Ce_xBr_3$ solid solution series are given in Table II, as determined by the endothermic peak temperature at which the rate of dehydration is greatest.

---

[9] G. Haeseler and F. MatthesA. Eisenberg, " Über den thermischen abbau der chloridhydrate der elemente der seltenen erden," *J. Less-Common Metals* 9(2), 133-252 (1965).

[10] W. W. Wendlandt, "Thermal decomposition of yttrium, scandium, and some rare-earth chloride hydrates," *J. Inorg. Nucl. Chem.* 5, 118-122 (1957).

[11] J. E. Powell and H. R. Burkholder, "The solubilities of lanthanum chloride 7-hydrate and lanthanum chloride 6-hydrate in water, and a study of the thermal decomposition of hydrated lanthanum chloride," *J. inorg. Nucl. Chem.* 14, 65-70 (1960).

Table 2. The decomposition temperatures (determined at1°C/min.) and melting points (3°C/min.) of $La_{1-x}Ce_xBr_3$ and their hydrates

Ce mole fraction $La_{1-x}Ce_xBr_3$	0.0	0.1	0.2	0.4	0.6	0.8	1.0
Decomposition of Heptahydrates (°C)	28.3	32.7	37.8	41.9	49	56.1	42.5
Decomposition of trihydrate (°C)	60.7	70.8	68	70.9	68.3	72.1	74.3
Decomposition of monohydrate (°C)	105.3	111.9	139.4	145.3	147.8	132.1	120.1
Melting point (°C)	773.7	760.7	764.9	756.0	746.0	734.6	722.4

These data indicate that the final dehydration temperature from the monohydrate to anhydrous powder in this binary system is below 145°C. Furthermore, the dehydration temperatures for $CeBr_3$ are greater than $LaBr_3$, which is consistent with dehydration behavior in other atmospheres.[14, 15, 16] However, the final dehydration temperature for $LaBr_3$ and $CeBr_3$ measured under a vacuum condition (105°, 145 °C) is much lower than that measured in air (210°, 240 °C)[15], in nitrogen (180°C, 220 °C)[13] and in argon ($LaBr_3$ ~250 °C), indicating the application of vacuum can effectively assist the dehydration process. Additional evidence has shown, after vacuum dehydration at 95C for several hours (> 6 hours) monohydrates can be converted to anhydrous powder. This observation is consistent with a small enthalpy change associated with phase change between monohydrate and anhydrous (see Fig. 3) and demonstrates vacuum can effectively assist the dehydration process.

(3) Structure and morphology evolution during vacuum dehydration

Fig. 4 is a scanning electron microscopy image of lanthanum bromide hydrate after the initial dehydration at 100°C in hot water bath for 3 hours. Prior to the vacuum dehydration, this powder consists of small heptahydrate crystals isolated from a supersaturated HBr solution from the direct acidification process (Eq. 1).

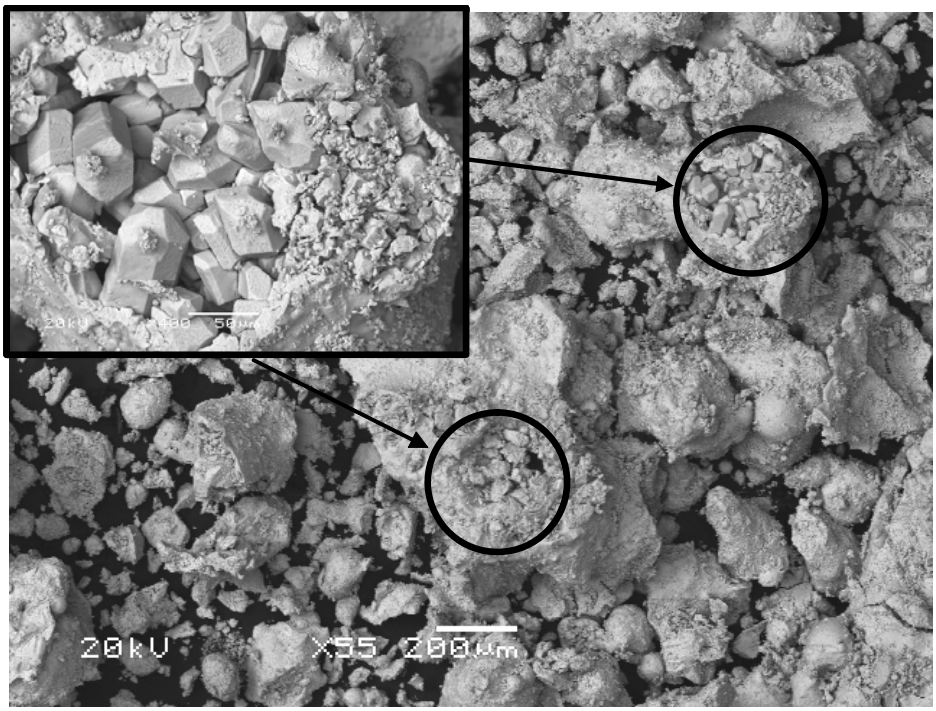

Figure 4. SEM microphotograph of partially dehydrated lanthanum bromide hydrates. Insert shows a cluster of $LaBr_3 7H_2O$ crystals.

The batch size for this dehydration experiment is large (~ 80 grams). The image indicates that during vacuum dehydration, the initial heptahydrate will dry and turn into agglomerated powder. This process happens at a temperature below 100 °C. If the powder agglomerate is crushed, partially dehydrated lanthanum heptahydrate bromide crystals (Triclinic, space group P-1) can be observed inside of the powder agglomerate with well defined facets (see insert in Figure 4). Therefore, the dehydration process starts from the outside and gradually turns hydrate into powder as bound water is removed from the surface. At this temperature (~100 °C), the dehydrated powder should have less bound water than the trihydrate form, based on data presented in Table I. These observations immediately suggest that under vacuum the heat transfer though a thick loosely powder in the Schlenk flask is poor, and can delay the decomposition reactions to a higher temperature.

To understand the structural evolution of the dehydration process, an *in situ* variable temperature *en vacuo* powder X-ray diffraction experiment was performed. In this process hydrated powder was placed on silicon (100) substrates and inserted into a vacuum (10^{-5} Torr) chamber for X-ray diffraction analysis. The sample was heated and diffraction patterns were collected at select temperatures. This was done for $\{[(H_2O)_7Ln(\mu\text{-}Br)]_2[Br]_4\}$, Ln = La and Ce. X-ray patterns reveal that the sample progresses through three separate phases: (A) crystalline hydrate, (B) apparently "amorphous" monohydrate (after the decomposition of trihydrate, based on TGA data in Figure 3), and (C) anhydrous $LnBr_3$, as the temperature increases. The structural evolution during dehydration for cerium bromide hydrate is given in Fig. 5.

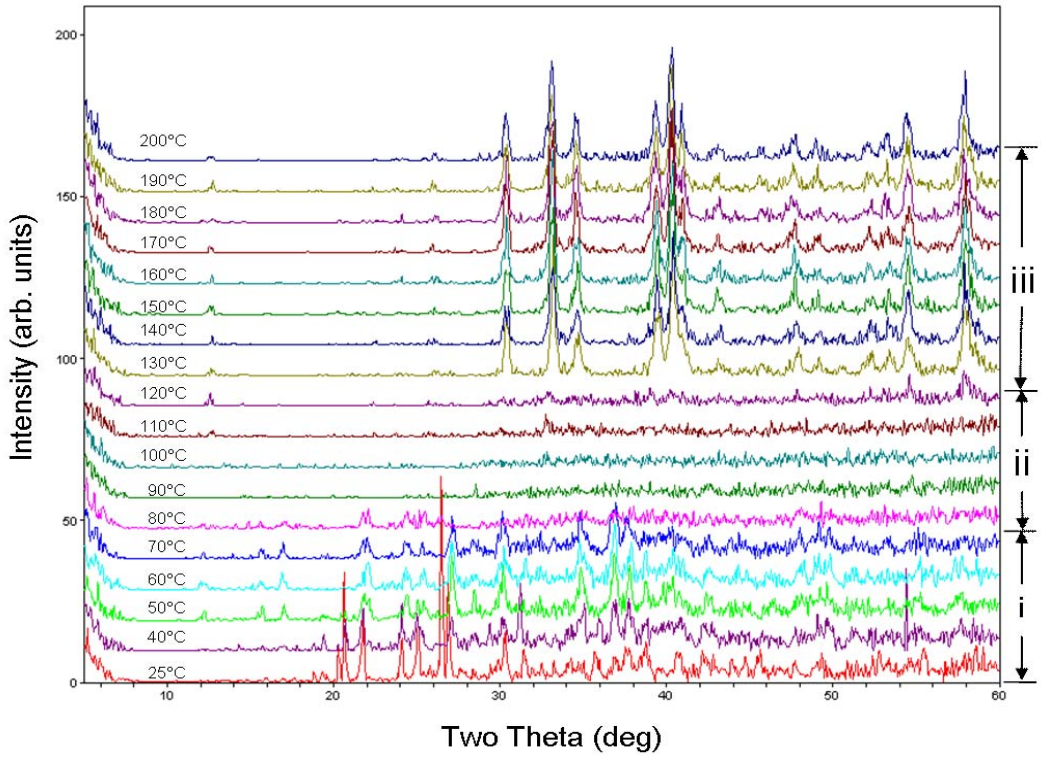

Figure 5. ***En vacuo*** **powder X-ray diffraction patterns illustrate the phase evolution during dehydration of cerium heptahydrate bromide including, (i) crystalline hydrates, (ii) "amphous" hydrates, and (ii) anhydrous $CeBr_3$**

Because the transition temperatures between crystalline and amorphous phases determined by the X-ray diffraction are consistent with the STA measurements (see Table 1), one can correlate the structural evolution during the dehydration. The crystalline structure of the hydrates is maintained during dehydration from the heptahydrate to the trihydrate, but is "lost" during the dehydration to the monohydrate as this unique set of diffraction patterns disappears. When the temperature is continually heated above 120 °C and the last bound water expelled from the amorphous monohydrate, the sample finally transforms to the anhydrous crystalline cerium bromide. However, crystalline hydrates such as trihydrate and monohydrate can be isolated when the dehydration temperature was held isothermally between two thermal events (or two endothermic peaks). The structure and phase transformation determined by the Be-D X-ray diffraction analysis from initial heptahydrate to anhydrous lanthanide bromide are tabulated in Table III. Details on the structural refinement of these hydrates will be presented elsewhere.[12] The results show that the conversion from initial hydrate to final anhydrous compound involves consecutive reconstructive phase transformations. The appearance of the "amorphous" pattern during the in-situ measurement could contribute to the kinetics of reconstructive phase transformations. The controversy between isothermal and continuous heating is further studied

[12] P. Yang, T. J. Boyle, M. A. Rodriguez, T. M. Alam, C. B. DiAntonio, M. R. Sanchez, and L. A. M. Ottley, "Vacuum Dehydratin and Solid Solution Formation of $LaBr_3$-$CeBr_3$," in preparation to be submitted to *J. Amer. Ceram. Soc.*, (2008).

by the structural evaluation of single crystal heptahydrate (see next paragraph). Quite unexpectedly, the X-ray diffraction data indicate that a complete solid solution between $LaBr_3$ and $CeBr_3$ forms after vacuum dehydration at temperatures below 200°C. The formation of a complete solid solution at such a low temperature is quite extraordinary.

Table 3 Structural phase transformations during the dehydration of $LaBr_3$ nH_2O.

Crystal Structure	Heptahydrate	Trihydrate†	Monohydrate	Anhydrous
Symmetry	Triclinic	Monoclinic	Orthorhombic	Hexagonal
Space Group	P-1	$P2_1$	Pnma	$P6_3/m$ (176)
a (Å)	8.1890(17)	12.480	5.910(2)	7.9723(6)
b (Å)	8.5587(18)	9.164	9.274(2)	
c (Å)	9.458(2)	7.339	11.201(2)	4.5149(5)
α (deg)	70.885(3)	90	90.0	
β (deg)	73.325(3)	92.6	90.0	
γ (deg)	81.468(3)	90	90.0	
Vol. ($Å^3$)	598.9(2)	840	614.4	248.51

† Possible cell structure for trihydrate, based on available data collected.

The differences observed in structural evolution during the isothermal and continuous heating and a poor heat transfer in vacuum dehydration suggest that the appearance of an “amorphous” structure during dehydration could be kinetically controlled by the reconstructive phase transformations. To obtain a clear picture, single crystal $LaBr_3$ heptahydrate was used with a low heating (1°C/min) and holding (10 minutes per measurement) to collect the structural evolution during the dehydration process. The results are shown in Figure 6. For clarity, Figure 6 only shows a limited range (5-35° 2θ). From this plot one can clearly see the change in diffraction pattern with dehydration. The 30 - 35 °C range shows signal consistent with the heptahydrate. The temperature range of 35 - 60 °C shows a new diffraction pattern which has been assigned as the $LaBr_3$ trihydrate phase based on TGA analysis. Continued heating above 60 °C shows the formation of a $LaBr_3$ monohydrate, again based on TGA analysis. Finally, we see the formation of $LaBr_3$ beginning at about 90 °C with full conversion to anhydrous $LaBr_3$ by 120 °C. The results for figure 6 track will with TGA analysis, confirm the multi-stage process of dehydration for this system, and demonstrate the importance of kinetics during the dehydration process.

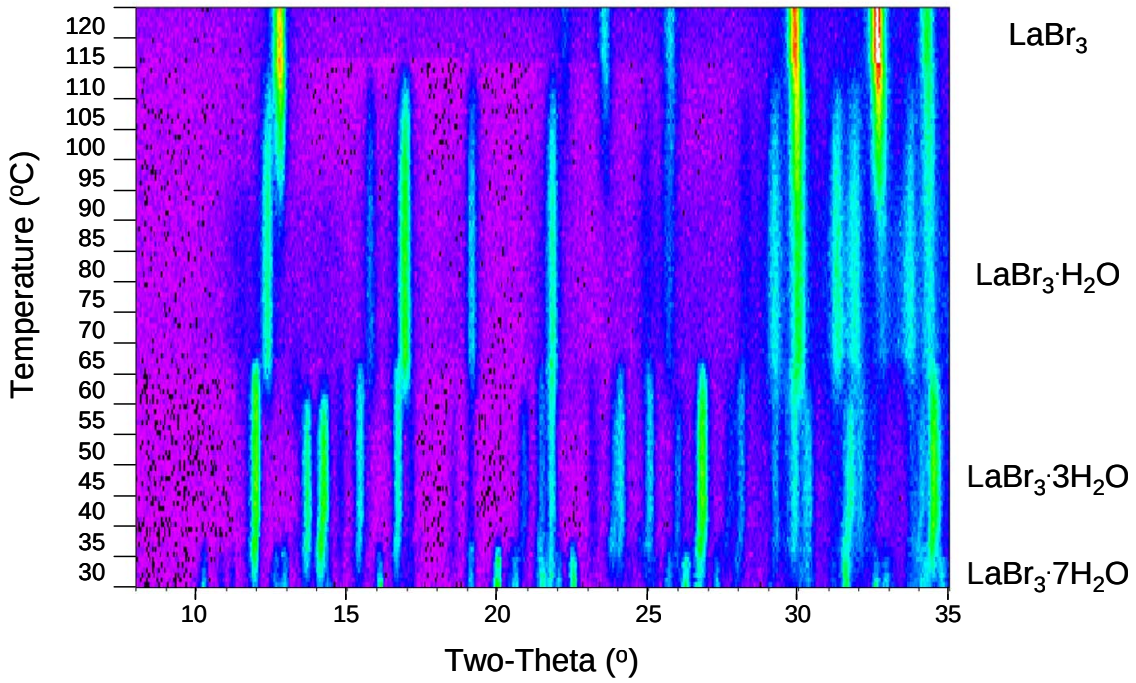

Figure 6. Contour plot of HTXRD showing dehydration of $LaBr_3$ $7H_2O$ with temperature. (Rainbow color scale, Red = high intensity, blue = low intensity).

After the powder has been ground and dried twice under vacuum at temperatures > 180°C for more than 6 hours, X-ray diffraction patterns were collected to examine the phase purity and to evaluate the possibility of bromine loss during dehydration. The diffraction pattern of a dehydrated lanthanum bromide and its calculated X ray intensity are given in Fig. 7. Measured lattice parameters (a = 7.972(2) Å, c = 4.507(1) Å, and V =248.1 $Å^3$) were consistent with literature values for the anhydrous $LaBr_3$. Results show that a proper dehydration can produce an anhydrous lanthanum bromide. In addition, within the X-ray detection limits the consistency in the measured and the calculated diffraction intensities for the anhydrous powder suggest that both lanthanide (La or Ce) and bromine sites are fully occupied after dehydration.

The anhydrous $LaBr_3$ powder is extremely hygroscopic. At the conclusion of this X-ray measurement, the Be-dome was removed from the holder. The thin layer of white $LaBr_3$ powder could be seen to immediately bow and flake upon exposure to the air (~ 10% relative humidity) in the laboratory. After 15 minutes of exposure to the ambient atmosphere, the powder was found to completely convert to $LaBr_3 7H_2O$.

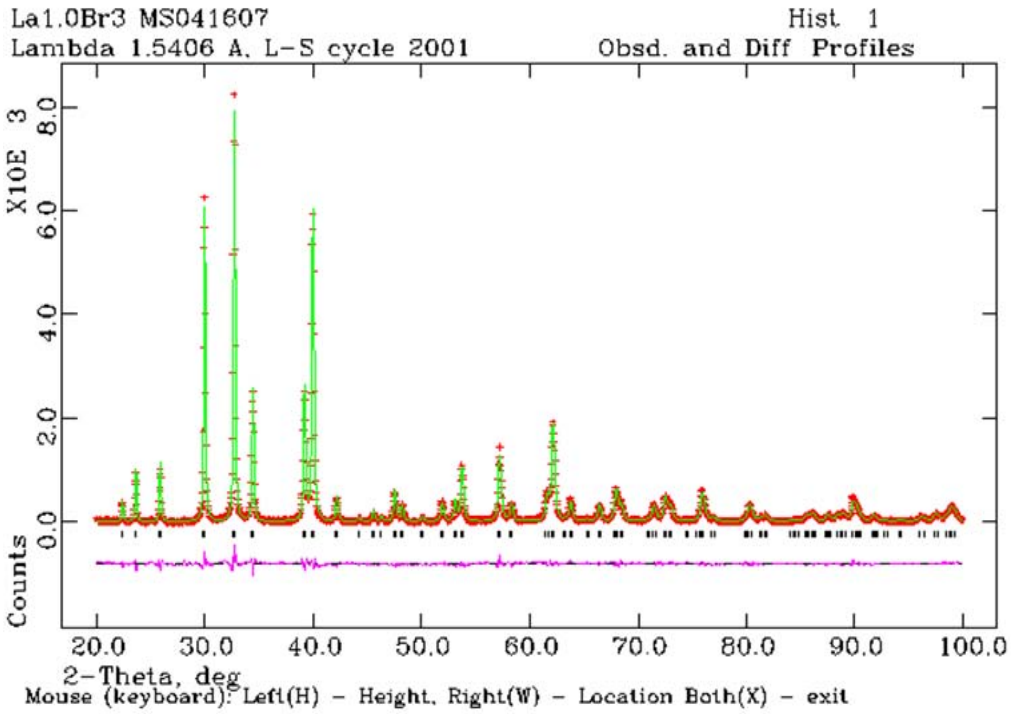

Figure 7. The measured (red cross) and calculated (line) X-ray intensities for anhydrous lanthanum bromide powder.

(4) $LaBr_3$-$CeBr_3$ binary phase diagram

The melting and freezing points for each composition in the $La_{1-x}Ce_xBr_3$ solid solution series were determined by the DSC measurement under flowing argon after dehydration (see data in Table 1). A binary phase diagram for $LaBr_3$-$CeBr_3$ is illustrated in Figure 8. The melting points, as determined at the peak temperature from the DSC curve, for $LaBr_3$ and $CeBr_3$ are 773 °C and 722 °C, respectively. These data are in good agreement with literature values[13] (i.e., $LaBr_3$: 786°C, and $CeBr_3$ at 732°C, respectively). The small anomaly on the melting curve for $La_{0.9}Ce_{0.1}Br_3$ in Figure 8 was repeatable. The data indicate that both the melting and freezing points generally decrease as the amount of Ce is increased in the $La_{1-x}Ce_xBr_3$ solid solution.

X-ray analysis indicates that cerium bromide has an identical crystal structure to lanthanum bromide, i.e., a hexagonal structure (space group $P6_3/m$ (No. 176)) with the a/c ratio greater than 1.76. This large c/a ratio and high thermal anisotropy (12×10^{-6}/°C along c axis, and 29×10^{6}/°C perpendicular to the prismatic plane)[14] pose a great challenge for growing large $LaBr_3$ single crystal of practical size for radiation detection applications. Details of the lattice parameters and unit cell volume in the $La_{1-x}Ce_xBr_3$ solid solution series are summarized in Table III. Results

[13] R. A. Sallach and J. D. Corbett, "Rare Earth Metal-Metal Halides Systems. V. Lanthanum, Cerium and Praseodymium Bromides," *Inorganic Chemistry* **2** [3] 457-459 (1963).

[14] P. Yang and F. P. Doty, unpublished data

shown there is a good linear correlation between unit cell volume (or c-axis) and $CeBr_3$ composition in the $LaBr_3$-$CeBr_3$ solid solution. From the melting behavior and structural change, it can be concluded that $LaBr_3$ and $CeBr_3$ can form a simple binary system. This is not a surprise since both compounds have the same crystal structure and the ionic size difference between these trivalent cations is small; therefore, a complete solid solution can be readily formed.

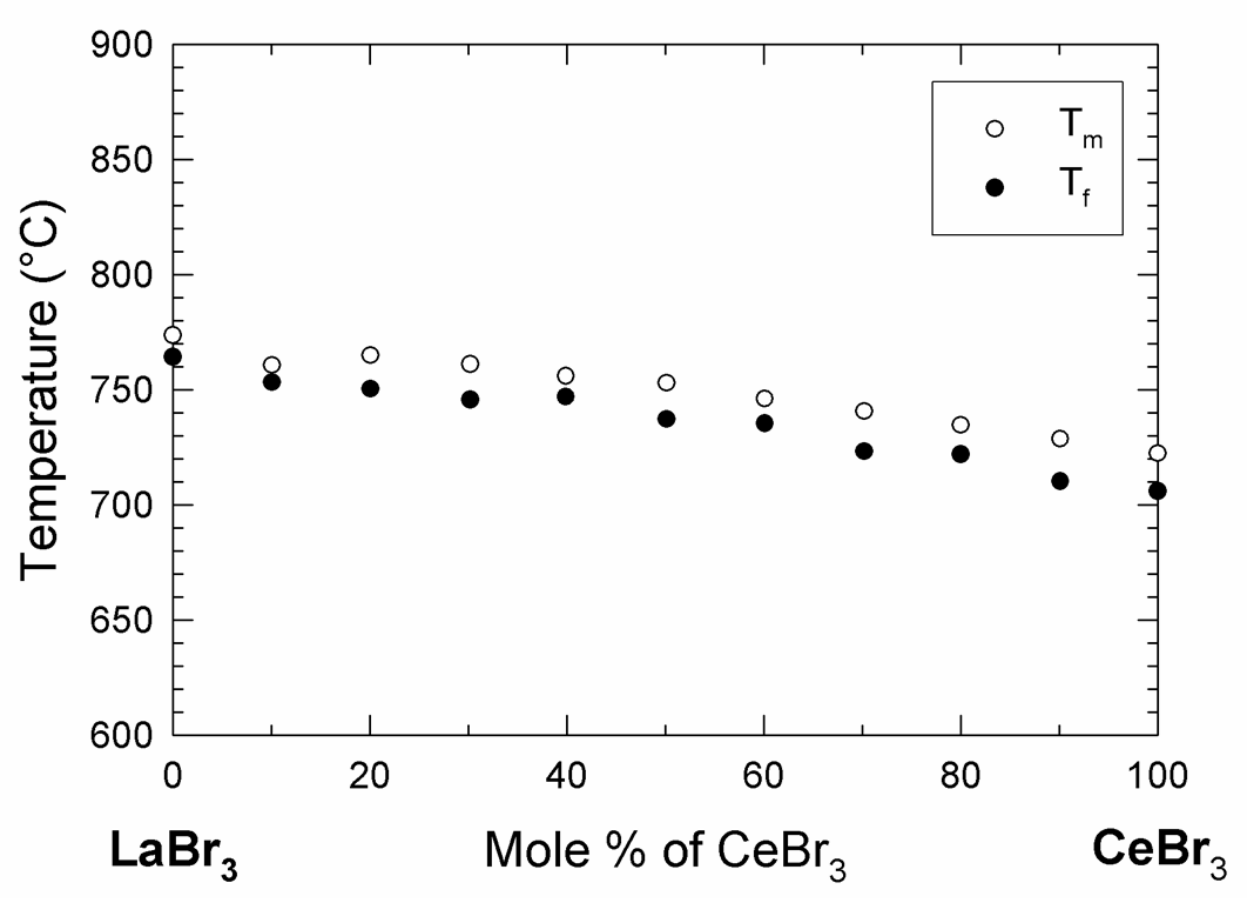

Figure 8. The phase diagram for the $Labr_3$-$CeBr_3$ binary system. The open circles and closed circles represent the melting and freezing points, respectively.

(5) Reduce foreign phase contamination and control dehydration process

Carbon contamination was proposed as the culprit for the darkening of chemically synthesized powder after high temperature thermal treatment during the Phase I development. The proposed mechanism was quickly discarded as the same phenomenon was observed after the synthesis process moved into a clean glovebox at the beginning of Phase II development. Since then work has been focused on potential water (or moisture) and oxygen contaminations, as well as the intrinsic thermal stability of the $LaBr_3$ compound.

The previous section has demonstrated that large batches of lanthanide bromide hydrates prepared by acidification of the bulk metal can be dehydrated to anhydrous crystals under vacuum. However, difficulties have been experienced with the complete dehydration of larger quantities of these hydrates (> 10 g). Part of the challenge comes from the effectiveness of heat transfer in a vacuum reactor. Another issue must also be attributed to the enthalpy requirement associated with the major events during the dehydration process (see Figure 3 for tri- and monohydrates). Due to the lack of convection heat-flow in a vacuum reactor, heat has to transfer through loosely packed powder from a hot surface, which can significantly reduce its effectiveness for the thermal dehydration of a thicker bed of powder. Material not in direct contact with the heated surface will only achieve partial dehydration. A good example is illustrated in Figure 4 where hydrate near the surface of agglomerates has turned into powder and partially dehydrated crystal clusters are preserved inside. Brown et. al.[15] has shown that a non-static vacuum approach seems to be effective in addressing this issue. Another challenge in assuring completely dehydrated, crystalline material is due to the difficulty in detecting the amorphous dihydrate and monohydrate by X-ray diffraction (see Fig. 5). If a trace amount of dihydrate or monohydrate remains, even an X-ray determined phase pure lanthanide bromide can turn into oxybromide when the powder is heated above 400 °C under flowing argon condition, according to the following hydrolysis reaction

$$LnBr_3 H_2O \rightarrow LnBr_3 + H_2O\ (vap.) \rightarrow LnOBr + 2\ HBr \qquad (2).$$

The validation of this proposed mechanism was one of the critical issues in the Phase II and Phase III development, as they might contributed to the LnOBr formation and subsequently darkening due to the reduction of $LnBr_3$.[16] This is manifested by the inconsistency in the amount of LaOBr phase present after same thermal treatment (at 720°C, 20 minutes in argon) of a single batch powder, where the amount of oxybromide varied from 3.9 wt.% to 30.6 wt.% between eleven experimental runs.[17] Furthermore, additional experiments using a fluidized reactor have shown to be effective in reducing the LaOBr formation below 4 wt.%. Particularly for powder dehydrated in the fluidized reactor below 500°C, the amount of oxybomide is below X-ray detection limits.[18] These evidences strengthened the proposed mechanism and demonstrated the importance of achieving a complete dehydration to prevent LaOBr phase formation. However, the assumption of the presence of residual hydrates after vacuum dehydration was proven to be incorrect later by NMR studies (see next paragraph) and directed our focus on powder handling in order to prevent moisture absorption on the powder surface.

---

[15] D. Brown, S. Fletcher, and D. G. Holah, "The Preparation and Crystallographic Properties of Certain Lanthanide and Actinide Tribromides and Tribromide Hexahydrates," *J. Chem. Soc.*, (A) 1889-1894 (1968).

[16] K. Krämer, T. Schleid, M. Schulze, W. Urland, and G. Mayer, "Three Bromides of Lanthanum: $LaBr_2$, La_2Br_5, and $LaBr_3$," *Z. Anorg. Allg. Chem.*, 575 61-70 (1989).

[17] P. Yang and T. J. Boyle, DNDO CFP06 TA-01-SL01 Annual Review Presentation at DNDO Headquarters, Washington D.C., December 4, 2007).

[18] P. Yang and T. J. Boyle, DNDO CFP06 TA-01-SL01, October, 2007 monthly report.

To verify the water retention of our anhydrous powder prepared by the vacuum dehydration process, NMR studies were undertaken using the ^{17}O isotope. Anhydrous $LaBr_3$ powder was dissolved in ^{17}O-labelled water (30% enriched H_2O*) and crystallized. The resulting crystals were dried, dissolved, and recrystallized two additional times. A sample of this material was set aside for analysis (Sample A). The remaining powder was dried at 200°C under vacuum (10^{-3} Torr) and another sample was set aside (Sample B). The rest of the powder was ground with mortar and pestle and then dried again in 200°C (Sample C).

The ^{17}O solid state magic angle spin (MAS) spectra were collected for these samples on a Bruker Avance 600 at 81.4 MHz, using a 4 mm broadband MAS probe. The spectra were obtained using a 10 kHz rotor spinning speed, with moderate 82 kHz ^{1}H TPPM decoupling. Results are shown in Figure 9 (a). The baseline spectra was obtained from H_2O^* (30% enrichment) which, as expected gives a narrow single resonance at δ =0.0. The spectra of first specimen (Sample A; $LaBr_3$ $7H_2O$) after three recrystallization process reveal 3 overlapping broad resonances (de-convolution and table are shown in Figure 9 (b)), which were assigned to H_2O^* species which is expected to give rise to a narrow spectra line but would be apparent in this region. After vacuum dehydration at 200°C (both Samples B and C), it was found that there was no ^{17}O MAS NMR signal observed at the NMR detection limits (< 100 ppt). To further support the argument that no water was present was present, Sample C was dissolved in toluene and the solution ^{17}O NMR spectrum collected, with no water signal being observed. Based on the ^{17}O H_2O spiking experiments, it can be argued that there is less than 100 ppm of water remaining in the dried material prepared by our vacuum dehydration process.

In addition, ^{139}La NMR data were obtained in MeOD-d_4. The ^{139}La chemical shift was found to occur at δ -37.5 ppm (Figure 9 (c)-i) and that of the dried material was found to be δ -34.7 ppm (Figure 9 (c)-ii). Titration of $LaBr_3$with aliquots of H_2O (15 μL aliquots in 500 μL MeOH total tube volume) show the conversion of $LaBr_3$ to the hydrate occurs rapidly with the ingrowths of a peak at δ -8 ppm (tentatively assigned to $La(OH)_x$) (Figure 9 (c) -iii). There was no indication of any resonance for $LaBr_3$ hydrate found in the spectrum of the dried material, again demonstrating that the drying procedure is complete in removing the bound water.

Since this only verifies the MeOD derivative is hydrate free, additional solid state ^{139}La spectra were obtained on the hydrate and dried material to verify the solid state materials are free of water. ^{139}La is a 7/2 spin nucleus with a considerable quadrupolar interaction. Based on literature, the QCC (quadrupolar coupling constant) would be between 15 and 30 MHz which would give rise to broad second order quadrupolar line shapes at the moderate field strengths used at SNL that could not be spun out even at superfast 35 kHz spinning. Therefore static spectra were obtained. Figure 10 (a) and (b) are the spectra obtained on the dry and hydrated samples. Figure 10 (a) shows the NMR ^{139}La spectrum for the $LaBr_3$. This line shape was expected based on previous literature, and was simulated with QCC = 17.4 MHz, η = 0 and a δ_{iso} = 418 ppm. A CSA of ~ 100 ppm has also been reported, but makes only a minor impact on the spectrum at this field. Figure 10 (b) shows the $LaBr_3$ • 7 H_2O ^{139}La NMR spectrum. The addition of O is expected to distort the local symmetry and increase the QCC. Previous literature for $LaCl_3$• 6 H_2O reported a QCC = 23.7 MHz, with η = 0.4. In general, this information is in agreement with the data presented in the literature and indicates that the $LaBr_3$•7 H_2O is analogous to the $LaCl_3$•6 H_2O and for $LaBr_3$ there is no water (at the less than ppm range).

(a)

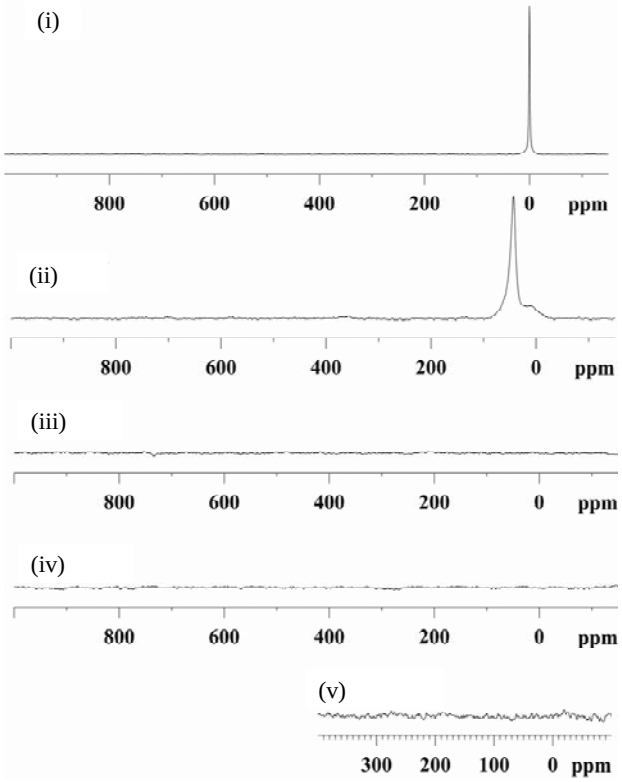

(b)

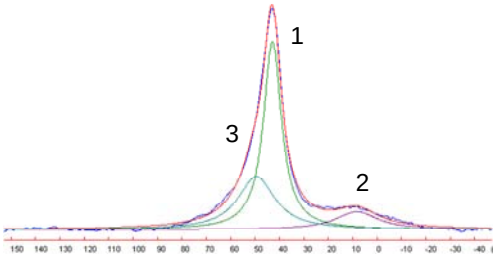

Barycentre 3304.36Hz / 40.60ppm

[a]Analytical integration accounts for different Gaus/Lor ratios

peak	Amplitude	Position (ppm)	Width (ppm)	xG/ (1-x)L
1	8937.25	42.84	8.92	0.00
2	843.72	8.28	21.36	0.00
3	2529.65	49.43	18.17	0.00
1	8937.25	3485.63	725.64	0.00
2	843.72	673.49	1737.64	0.00
3	2529.65	4021.51	1478.08	0.00

	Analytical Integration[a]	Model Integration	
	% integral	%	Intensity
1	55.48	56.42	9894870.07
2	12.54	12.03	2109031.86
3	31.98	31.55	5534026.13

(c)

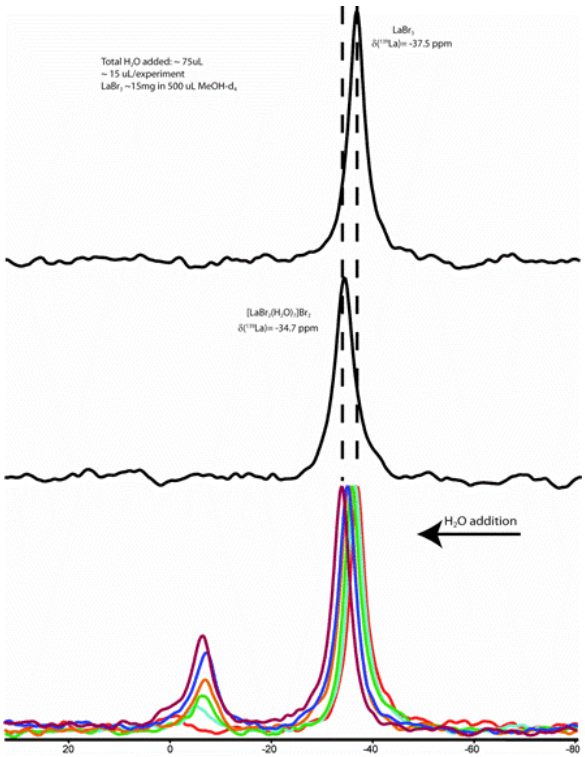

Figure 9 (a) Solid state ^{17}O NMR spectrum of (i) H_2O*, (ii) $LaBr_3$•$7H_2O$*, (iii) $LaBr_3$•$7H_2O$* dried at 100°C (iv) $LaBr_3$•$7H_2O$* dried at 200°C and (v) solution state of ^{17}O NMR spectrum $LaBr_3$•$7H_2O$* dried at 200°C in tol-d_8. (b) deconvolution of $LaBr_3$•$7H_2O$* , and (c) ^{139}La NMR spectrum of (i) $LaBr_3$, (ii) final $LaBr_3$•xH_2O, and (iii) titration of $LaBr_3$ with H_2O.

These analytical efforts demonstrated that our vacuum dehydration effectively removes residual water and the water contain in the produced anhydrous powder is below NMR detection limits (< 100 ppm). The source of oxyhalide formation was thought to be from the powder handling process due to the hygroscopic nature of $LaBr_3$. This hypothesis was evaluated by a series of melting experiments in sealed quartz ampoules. In these experiments, samples from commercial source (identified as F powder; not shown) and Sandia process (vacuum dehydrated powder, A to E) were vacuum sealed (10^{-3} Torr) in quartz tubes and heated to 823° C, above the $LaBr_3$ melting point (~778°C), to examine the effect of processing and handling on the darkening issue. Sandia powders, which were fully dehydrated (A and B) and briefly exposed to ambient conditions (C and D), as well as with the addition of a few drops of liquid bromine (E), were vacuum sealed in individual quartz tubes before thermal treatment. Samples were heated to 823°C and held for 2 hours after they had completely melted, then slowly cooled through the melting point (0.1°C/min) and finally furnace cooled to room temperature. The results of these melted samples are given in Fig. 11 (A), where above the melt (now solidified) darkened material was observed for all samples. A similar behavior was observed on commercial powder. XRD later confirmed that the dark material collected above melt and solidified material from ampoules (A), (B) and (E), were anhydrous $LaBr_3$:Ce^{+3}. Differences between the dark and solidified materials were beyond XRD detection limits. For samples (C) and (D), instead of the

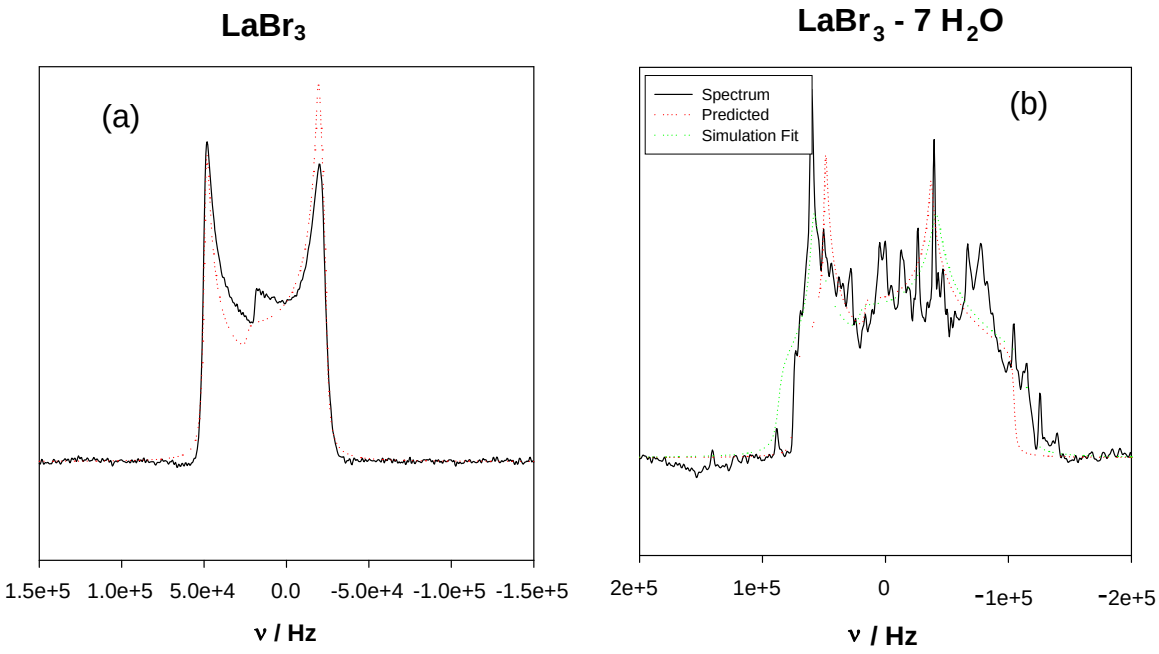

Figure 10. ^{139} LaNMR solid state (static) spectrum of (a) LaBr3 and (b) LaBr3 • 7 H2O: black experimental spectrum, red predicted, blue simulated.

darkened material, an additional white deposit was found above the melt and a few clear droplets (see Fig.11 (B)) were condensed on the top of the ampoules, confirming that carefully controlled processing and handling conditions are critical to producing anhydrous powder. The white deposit was confirmed to be LaOBr (pure LaOBr is white color). Furthermore, the formation of the darkened material after melting suggested that darkening might be thermally induced from the intrinsic stability of the $LaBr_3$.

With this evidence, a rigorous process control was implemented in Phase III development, in which all the powder synthesis and dehydration were performed in an argon filled glovebox. Anhydrous powder was sealed in glass jar and transferred to an argon purged box for high temperature densification. XRD results have shown that samples after densification had no oxybromide.

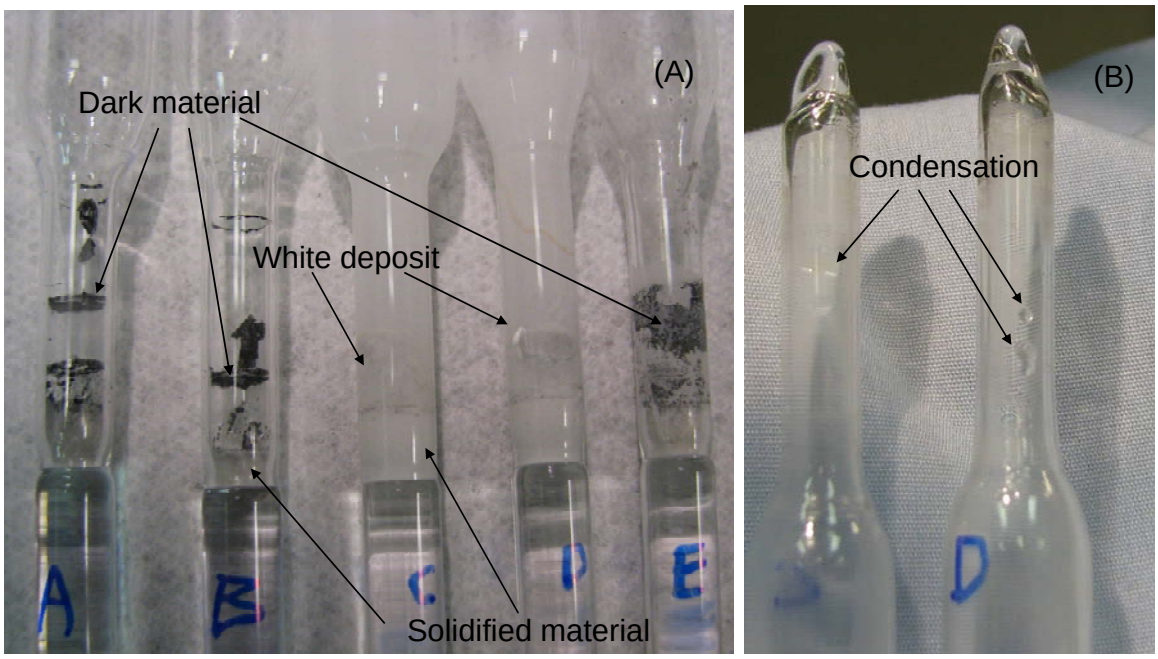

Figure 11. Melting experiments for Sandia synthesized $La_{0.95}Ce_{0.05}Br_3$ power under different condition. Details of these powders are described in the text. (A) Samples located at the bottom of quartz ampoules, (B) condensation observed on the top of quartz ampoules after melting.

(6) The intrinsic thermal stability of fine $LaBr_3$ powder

The melting experiments presented in the previous section suggest the intrinsic thermal stability could be the reason for darkening the powder after high temperature processes. The difference in the appearance for the dark anhydrous $LaBr_3$:Ce^{+3} on top and the solidified, translucent material at the bottom of the ampoules indicates that material near the solid-vacuum interface could be unstable as bromine becoming volatile at high temperatures. However, verification of this assumption by analytical measurements, including X-ray diffraction, electron microprobe analysis (EMPA, no suitable standards), X-ray photospectroscopy (XPS) measurements, and induction coupled plasma atomic emission spectroscopy, was challenging because each method has its own limitations in providing quantitative results on structural defects developed at high temperatures, particularly when the focus is on the surface layer. We have systematically removed the possibilities of carbon contamination and residual hydrates for the cause of darkening. A previous thermal gravitation analysis[5] (TGA) showed that the weight loss started above ~340°C and continued to its melting point for single crystal $LaBr_3$ and commercial powder, where powder lost more weight than single crystal specimen. The observation was confirmed when comparing results between the commercial powder (~1 mm diameter beads) with Sandia powder (see Figure 12), where chemically prepared powder with larger surface area lost more weight than the commercial powder. These observations suggested that the surface layer on the $LaBr_3$ powder was thermally unstable at high temperatures. Lattice defects and color centers can be created as bromine becomes volatile at these temperatures. These defects in turn produce a darkening effect after thermal process. It is, therefore, possible that commercial

vendors normally produce $LaBr_3$ beads instead of fine power to minimize the surface area and avoid this undesired effect. However, these results cannot explain the observed an exothermal event between 336°C and melting point, detected by the differential scanning calorimetry (DSC). Further analysis is required to obtain a better understanding of this subject.

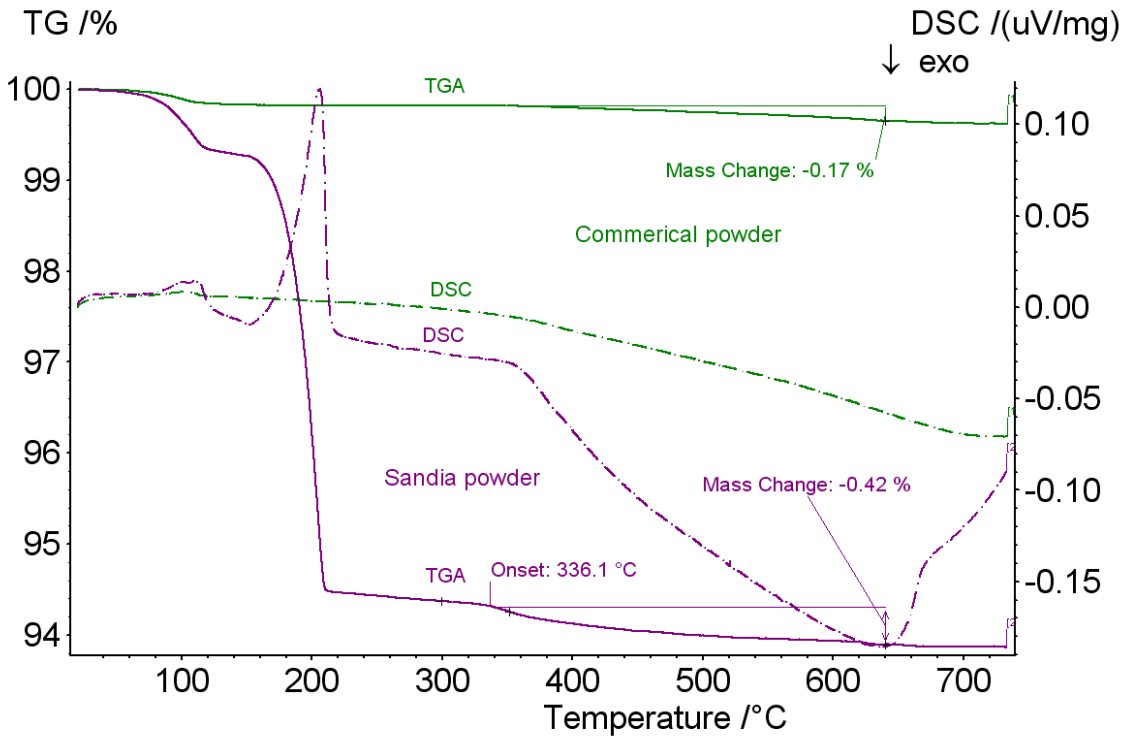

Figure 12. Simultaneous thermal analysis (STA, including TGA (solid lines) and DSC (dotted lines)) for a commercial powder (in green) and a vacuum dehydrated powder (in purple) prepared at Sandia.

(7) Water-free synthesis routes

At the end of Phase I development, we were unable to yield oxyhalide free powder. This led to the development of alternative methods to generate oxygen-free $LaBr_3$. Figure 13 shows the crystallographic pathway for the dehydration methanolation of $LaBr_3$. Using commercially available non-dense $LaBr_3$ (C), it was discovered that dissolving $LaBr_3 \cdot 7H_2O$ in MeOH an unusual salt was formed that consisted of a partially substituted $LaBr_{2.75}/LaBr_{3.25}$ MeOH substituted species (E). This was easily converted to $LaBr_3$ fully dense by heat treating under vacuum.

Attempts to replicate this from the $LaBr_3 \cdot 7H_2O$ at room temperature led to the isolation of a partially substituted $MeOH/H_2O$ species B; however, at reflux temperatures, the conversion is complete, yielding E, the 2.75/3.25 salt. This is in agreement with the NMR data shown in Figure 9 that shows an increase in temperature increases the conversion of MeOH for H_2O. Interestingly, the conversion of the $LaBr_3 \cdot 7H_2O$ that had been dried at 200 °C under vacuum upon exposure to MeOH led to the fully inner sphere bromide MeOH derivative (D). Efforts to

convert this to the anhydrous species at 500 °C were successful. Details of this synthesis route are reported elsewhere.[19]

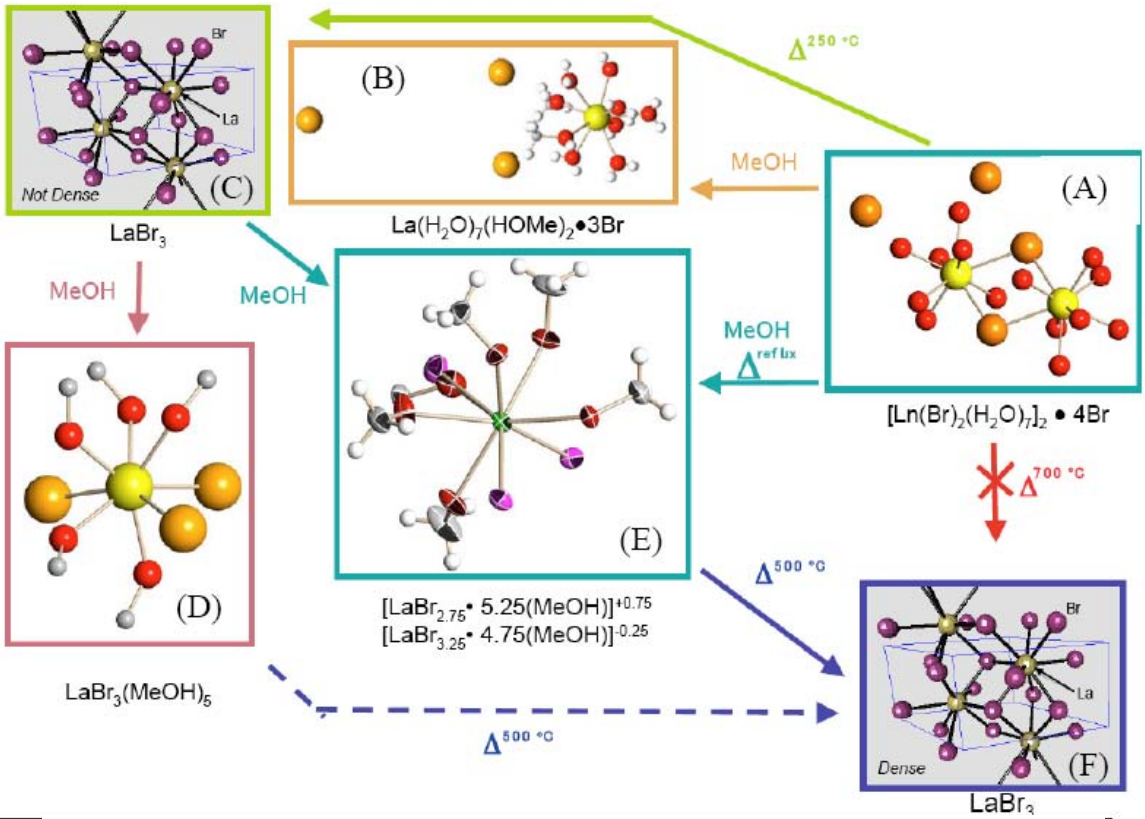

Figure 13. Crystallographic characterized conversion of $LaBr_3$ $7H_2O$ to fully anhydrous $LaBr_3$ though MeOH substitution.

Alternatively, using liquid ammonia would allow for oxide free species to be produced. Dissolution of the $LaBr_3$•$7H_2O$ in NH_3(l) led to a XRD pattern that resembles NH_4Br. This is not surprising since the outer sphere Br is present and potentially coordinates NH_3. Heating of this appears to form LaOBr; however, Reitfeld analysis indicates the majority of these anions may be N not O. Processing by firing under an argon atmosphere yielded LaOBr. These preliminary results called a halt to the further investigation in this synthesis route.

In conclusion, the vacuum dehydration process is effective to lower the processing temperatures in comparison to those processed in air or in a nitrogen atmosphere. The $LaBr_3$ and $CeBr_3$ solid solution can be readily formed at temperatures below 200°C. The dehydration involves a reconstructive crystalline-amorphous-crystalline phase change as bound water is progressively removed from the hydrate. Results show that these anhydrous compounds form a simple $LaBr_3$-$CeBr_3$ binary phase system, as determined by thermal analysis. Incomplete dehydration can lead to the formation of oxybromide. Anhydrous powder has to be handled in a rigorous process to prevent moisture absorption at powder surface. The intrinsic thermal stability of these lanthanide

[19] T. J. Boyle, L. A. M. Ottley, P. Yang, T. M. Alam, M. A. Rodriguez, "Methanolation of lanthanum Bromide Hydrate," Submitted to *Inorg. Chemistry* (2008).

halide compounds gives an ultimate challenge in fabrication of optical quality, ceramic scintillators from a chemically prepared, ultra-fine powder.

2.1.2 Task 2: Lanthanum halide seed particle synthesis

2.1.2.1 Development Approach

High aspect–ratio seed particles used in this investigation play two important roles in the final process to create highly textured ceramics that will significantly reduce the amount of light scattering in birefringent materials such as lanthanum halides. First, when incorporated with fine ceramic powder, the longer dimension of these highly anisotropic seed particles will be aligned in the shear direction with help from a localized shear stress. Second, under proper thermal conditions, these large seed crystals grow faster than the surrounding fine powder. They therefore consume the fine powder and convert the original unfired ceramic body (or green body) into a dense, preferentially assembled microstructure in a polycrystalline ceramic body. Seed particles with desirable morphology and size are not commercially available, and information about the synthesis process is not available in the literature. In process development, we have focused on approaches that are simple, effective, and controllable to consistently produce seed particles with desirable morphology and reduce total manufacturing costs.

2.1.2.2 Development Details

(1) Characterization of seed crystals synthesized from tetrahydrofuran (THF)

In the first Phase development, large (> 100 μm), highly anisotropic seed crystals were synthesized from tetrahydrofuran (THF) by a hot solution method. These particles exhibit cathodoluminescence under an electron beam.[5] However, these seed particles exhibited thermal stability issues when incorporated in ceramic during densification process.[5] This led a detailed studies on the structural evolution during the thermal process. Transmission electron microscopy (TEM, see Figure 14) of the single crystal seeds shows that the large rectangular plates become unoriented nanocrystalline aggregates after thermal treatment (or stabilization process[5]), and there is a carbonaceous layer about the perimeter. This carbon layer actually prevents hydrolysis of the $LaBr_3$ crystals, but the impact of the carbon on the optical properties cannot be overcome. In retrospect, the change from large crystals to nano-aggregates was not a surprise as it was similar to the evidence found in the reconstructive phase changes inform the dehydration process and NH_3 substitution experiments. The observation made a major change in our seed particle synthesis strategy. To overcome the technical challenge resulting from the adsorption of solvent molecules in seed particles formed by solvent based recrystallization, new approaches such as vapor phase synthesis.

(2) Vapor phase transport for $LaBr_3$ seed crystal synthesis

A vapor phase transport process was developed to produce $LaBr_3$ seed crystals using $AlBr_3$ as a complexing agent according to the following reaction equation.

$$LaBr_3(s) + \tfrac{n}{2} Al_2Br_6(g) = LaAl_nBr_{3n+3}(g) \qquad (3)$$

Jiang et al. have used this type of reaction with the rare earth chlorides for separation activity using Sc, Y, and La rare earths[20]. Adachi et al. have developed this method for separation of Pr, Er and Nd as well[21]. Prior work in this field has tended to focus on the chloride materials, and the formation of gaseous species using either Al or Fe chlorides as complexing agents[22]. Both these chlorides are typical examples of Lewis acids, and Emmenegger states that complex formation

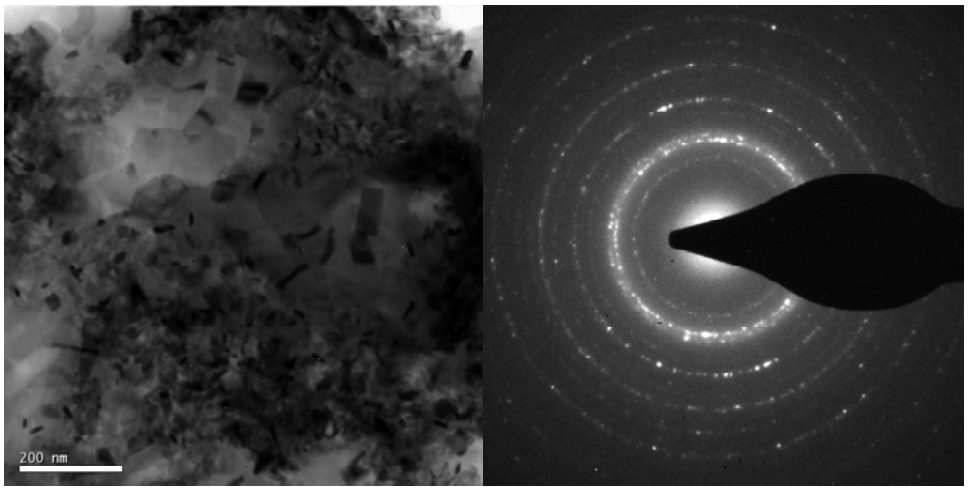

Figure 14. TEM microphotograph illustrated after the forming gas treatment, a large seed particle becomes unoriented nanocrystal aggregates. The lattice spacings determined by the selective area diffraction are consistent with anhydrous $LaBr_3$.

may be considered as an acid-base interaction. We have seen crystal formations, growing on the alumina crucible surface, during attempts at heat treatment of the materials synthesized for this program. Therefore, it should be a promising research study to look at the formation of crystals using vapor transport, and to consider the effect of $AlBr_3$ as a complexing agent to raise the mass transport of the desired $LaBr_3$. These studies also use active carbon to remove oxygen from the furnace process, but the definition of active carbon remains unclear. This may not be necessary in this system, as Kramer et al. show that aluminum bromide has been used to form lanthanum bromide from an oxide starting material by the reaction equation.[23]

$$La_2O_3(s) + 3Al_2Br_6 = 4LaBr_3 + 6AlOBr \qquad (4)$$

We will not use $AlCl_3$ in the system, as Schulze and Urland report a method for forming mixed rare earth chloride-bromides by using a combination of $AlBr_3/AlCl_3$.[24]

---

[20] J. Jiang, T. Ozaki, K. Machida, G. Adachi, *J. Alloys Compounds* **264** (1998) 157-163.

[21] G. Adachi, K. Murase, K. Shinozaki, and K. Machida, *Chem. Lett.* (1992) 511-514.

[22] F. P. Emmenegger, *J. Cryst. Growth* **17** (1972) 31-37.

[23] K. Kramer, T. Schleid, M. Schulze, W. Urland, and G. Meyer, *Z. anorg. allg. Chem.* **575** (1989) 61-70.

[24] M. Schulze and W. Urland, *Eur. J. Solid State Inorg. Chem.* (1991) 571-574.

The process uses the vapor phase generation of $AlBr_3$ at an initial low temperature stage (~200 °C) to create the complex vapor species and species given by Eq. 3 at the higher temperature of 800-1000 °C over molten $LnBr_3$. The temperature range for optimal production will have to be determined, as Kramer performed crystal growth in a two stage furnace set to 400 °C and 500 °C. The reverse reaction of Eq. (4) occurs on cooling of the thermal profile of the furnace. We have observed the decomposition of $LaBr_3$ at temperatures over ~800 °C. A carrier gas of nitrogen and bromine is necessary to prevent thermal decomposition of the $LaBr_3$ (flow rates are 30-35 ml/min). Excess bromine gas species drive the chemical equilibrium toward the formation of $LaBr_3$. Previous work has used HBr or NH_4Br gases. Kramer et al. stated that using ammonium bromide as the carrier gas produced a powder, whereas aluminum tribromide results in the observation that the "…growth of single crystals of $LaBr_3$ can hardly be avoided."

Initial trials were performed by mixing the aluminum and lanthanum bromides together and reacting them in the center of the furnace at 570 °C. Crystal production was prolific outside of the furnace zone. However, SEM and energy dispersive spectroscopy (EDS) analysis showed that these crystals were aluminum bromide. Reasons for this finding are suggested to result from the low vapor pressure of lanthanum bromide at 520 °C (0.0006 mmHg) and the evaporation of the aluminum bromide, which melts at 97.5 °C, and creates a vapor pressure of 1 torr at 81 °C (shown in Figure 15). This results in preferential transport of the aluminum bromide. By using the complexing agent $AlBr_3$, we were able to increase the $LaBr_3$ pressure to the equivalent level as the $AlBr_3$, without actually heating the $LaBr_3$ to the temperature at which its normal vapor pressure would be equal. The $AlBr_3$ forms a complex in the vapor phase, which in turn reduces the vapor concentration of the $LaBr_3$, so the solid phase is induced to evaporate more. The result will be additive - the vapor pressure of $LaBr_3$ at that temperature plus the vapor concentration of the $AlBr_3$-$LaBr_3$ complex (which will depend on the temperature of the $AlBr_3$ solid at the start of the furnace). If the $AlBr_3$ is heated to 56 °C, the problem becomes a matter of investigating the temperature to hold the $LaBr_3$ source to produce good crystals. That temperature should be less than the 765 °C, but is still unknown. The critical reaction parameter will be the rate of formation of the complexed gaseous species from the solid $LaBr_3$ to the vapor phase. Most references suggest a temperature difference of 500 to 400 °C for the lanthanum bromide crystal growth.

Additional testing was performed using the aluminum bromide in a boat at the entrance of the furnace to keep the temperature below its melting point (~97°C), and a separate boat with lanthanum bromide located in the hot zone of the furnace. Treatments were conducted under flowing argon atmosphere. These tests were performed using a temperature of 760 °C in the hot zone, with the $AlBr_3$ halfway outside the tube. This temperature caused discoloration, attributed Additional testing was performed using the aluminum bromide in a boat at the entrance of the furnace to keep the temperature below its melting point (~97°C), and a separate boat with lanthanum bromide located in the hot zone of the furnace. Treatments were conducted under flowing argon atmosphere. These tests were performed using a temperature of 760 °C in the hot zone, with the $AlBr_3$ halfway outside the tube. This temperature caused discoloration, attributed to decomposition of the aluminum bromide. Operation at 590 °C was also characterized by formation of aluminum bromide crystals. The $AlBr_3$ was placed outside the furnace heating zone as far as possible, and it was found that the material did not decompose. White crystals were found at the exit of the furnace tube and are under investigation. An additional test is in progress

using a bromine source to attempt to prevent decomposition of the bromides in the furnace, and will be described as information becomes available.

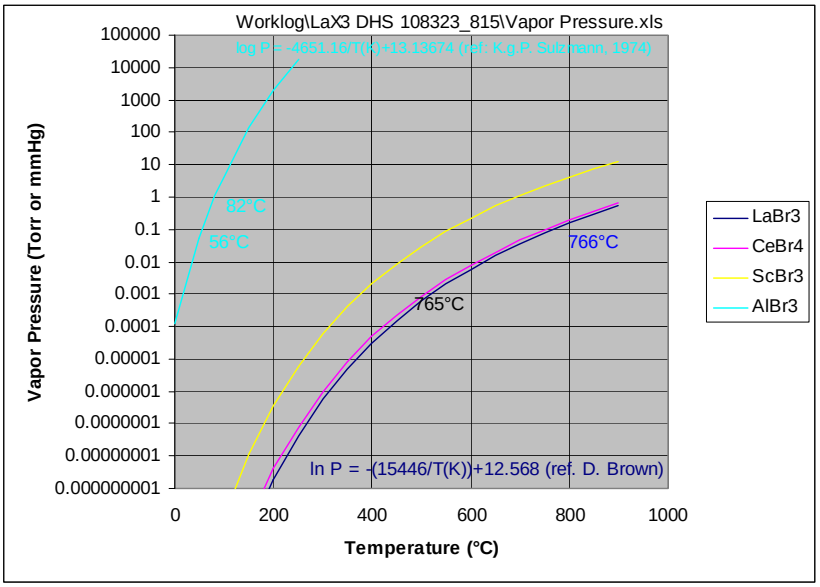

Figure 15. Vapor pressure of aluminum bromide and rare earth bromides vs. temperature.

Several reactor configurations were explored; one double-tube configuration showed that $LaBr_3$ seed crystals were deposited at an undesired location near the reactor entrance, which made them difficult to retrieve without exposure to atmosphere. However, these seed particles have a platelet morphology and good purity, based on EDS analysis (see Figure 16). $LaBr_3$ seed crystals isolated from the other configuration (500°C for 48 hours), using a closed quartz tube system to enrich the complexing agent concentration and to increase the deposition rate, exhibited a significant amount of silicon contamination, presumably due to a chemical reaction between quartz tube and highly corrosive bromine gas at the high temperature.

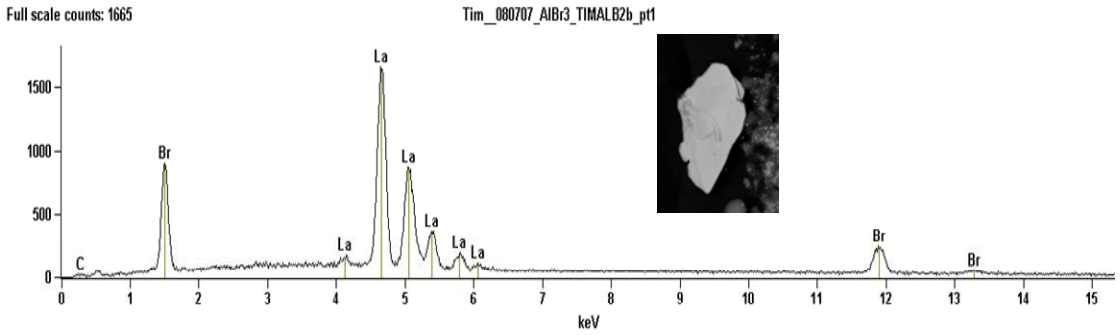

Figure 16. The EDS results of seed crystals obtained from a double-tube quartz tube reactor.

Based on these results, a two-thermal-zones setup with an alumina tube reactor was explored to minimize the silicon contamination. Figure 17 shows the reactor and furnace where the $AlBr_3$ and $LaBr_3$ powder mixture was placed near the round sealed end of alumina tuber with temperature set at 500°C on the right, $LaBr_3$ seed crystals were deposited and grown on the alumina tube in the low temperature furnace (300°C) on the left (near the furnace entrance). As both zones reach their set points, bromine gas was introduced into the reactor through Tygon tubing (after exposures to bromine gas these tubes turn red color). The open end of alumina tube was sealed with a rubber stopper wrapped with Teflon tape (white color) to prevent undesired chemical reactions at high temperature. Our first trial run showed that even at temperature lower than 300°C bromine has reacted with rubber (through the Teflon tape). A Teflon fixture was designed to replace the rubber stopper. At that time (after the second quarter review in FY07), program manager at DNDO TRDD, Dr. Alan Janos, has decided to focus our development effort on the darkening issue observed during the high temperature process instead of on seed crystals.

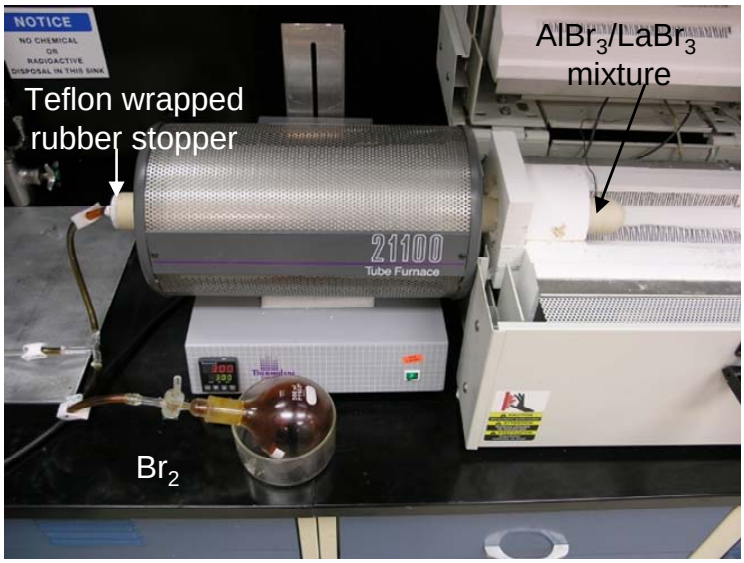

Figure 17. The two-zone vapor phase transport alumina reactor for $LaBr_3$ seed crystal growth.

2.1.3 Task 3: Texture development and densification

2.1.3.1: Development approach

Fabricating transparent ceramics is a challenging task. This is especially true when dealing with birefringent materials such as lanthanum halides since the amount of light scattering at grain boundaries in a polycrystalline ceramic is proportional to the square of refractive index difference between different optical axes. Traditionally, ceramic engineers control the microstructure in a polycrystalline ceramic body to a submicron range to achieve high transparency (for example, transparent alumina tubes[25] used in high pressure sodium lamps).

Recent research has shown that the use of hot pressing to align the crystallographic orientation of individual grains for an optically anisotropic material enables fabrication of index matching grain

[25] R. Apetz and M. P. B. van Bruggen, *J. Am. Ceram. Soc.*, **86** [3] 480 (2003).

boundaries and yields transparent ceramics for hydroxyapatitie.[26] Using a refractive index of 1.92, an index difference of 0.02, and a wavelength of 360 nm, a theoretical value of particle size of less than 7.0 nm is needed to allow a totally random lanthanum bromide ceramic to achieve a light scattering below 3%/cm, according to a first-order calculation (van de Hulst, 1981).

The small grain size poses a great processing challenge for ceramic engineers since a typical sintering process produces grain sizes ranging from 0.5 microns to several tens of microns. Therefore, our first attempt focused on the development of highly textured lanthanum halide ceramics. We reserved the use of the ultrafine grain approach as a risk mitigation plan, as discussed in the original proposal.

2.1.3.2: Development details

At the beginning of Phase II, we quickly learned that seed crystals grown from a hot THF solution can not be used to induce crystallographic texture in a ceramic body as these crystals turned into nanocrystalline aggregates at high temperatures and lost their template function. At the same time, we frequently broke our alumina dies during hot pressing as they are prone to fracture under high pressure. As a result, developing an alternative approach that can improve the densification and texture development became a major thrust. This effort led to the development of an Inconel 718 super alloy die. The super alloy die (1.25" ID) worked with a copper foil liner to prevent chemical reactions between the metal alloy and $LaBr_3$ at high temperature and high pressure conditions. Inconel was chosen because of its high temperature strength which effectively doubled the applied pressure from ~ 5 kpsi (graphite) to ~ 10 kpsi (Inconel) at temperature above 680 °C, and it can be used in a reduced atmosphere (vacuum or argon). The design permits this super alloy die to sustain a maximum pressure of 10 kpsi (with an additional 75% safety margin). This new capability had proven to increase our processing window and enhance the densification process. In addition, abnormal grain growth and pressure induced texture development were observed in the hot pressed $LaBr_3$ under high pressure conditions.

In Phase III, powder handling took precedence to overcome the process inconsistency observed in the Phase II program. During previous hot pressing runs, powder compacts would experienced a brief time exposure (<10 minutes) to ambient air during the set-up procedure. The exposure could result in the formation of hydrates which might turn into oxyhalide (even in an oxygen-free condition) at high temperatures. To prevent the exposure to the moisture, powder compacts should be constantly handled in an inert atmosphere. Thermal processes such as sintering or hot pressing would be performed in an oxygen-free condition to reduce the oxyhalide formation. This led to the development of an in-house-atmosphere-controlled hot pressing capability, where powder compacts were transferred in a sealed can from an argon-filled synthesis glovebox to another argon-filled thermal processing glovebox.

(1) Densification, post-thermal treatment, and texture development

Powders from different sources, including commercial $LaBr_3$ powder, Sandia synthesized $La_{0.95}Ce_{0.05}Br_3$ powder, and LANL melt spinner $La_{0.95}Ce_{0.05}Br_3$ powder (see equal channel angular consolidation section for details), were hot pressed at 740°C in vacuum under different

[26] Y. Watanabe, T. Ikoma, A Monkawa, Y Suetsugu, H. Yamada, J. Tanaka, and Y. Moriyoshi, *J. Am. Ceram. Soc*., **88** [1] 243 (2005).

pressure conditions. All pellets after longer pressing time (> 12 hours) turned dark (see insert photo in Figure 18(a)). A short pressing time (1 hour) produced a light grey color pellet similar to our previous observation. However, after a post treatment at 720°C under a flowing bromine/Ar condition, the sample converted back to a white color (insert photo in Figure 18(b)). XRD indicates that the post-thermal treated sample is phase pure $LaBr_3$ (Figure 18). This observation immediately suggests that some bromine might have lost during high temperature process, and under a bromine rich condition the lattice defects that cause the darkening of lanthanum bromide (could be La_2Br_5; black color, but has not been detected by XRD) can be annealed out and revert back to $LaBr_3$. This is consistent with the thermal instability argument causing the darkening behavior for chemically prepared, ultrafine $LaBr_3$ powder.

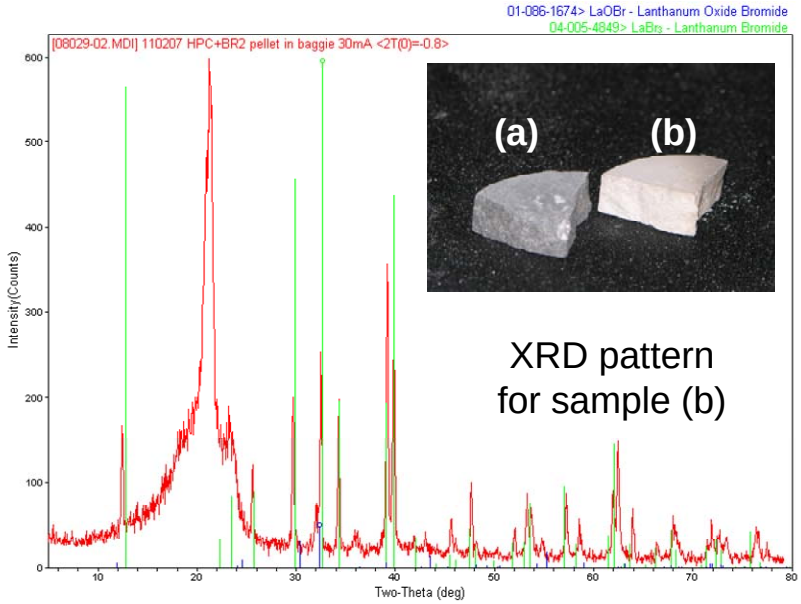

Figure 18. X-ray diffraction pattern for the thermally treated hot pressed $La_{0.95}Ce_{0.05}Br_3$ ceramic (5 kpsi at 740°C, 24 hours) under a flowing Br_2/Ar condition (720°C, 3 hours). The insert photos show the color difference of hot pressed ceramic before (a) and after (b) bromine gas treatment.

Hot pressing of fine grain $LaBr_3$ powder at 10 kpsi has also been explored with our new Inconel 718 die. The first experiment was run at 740°C for 12 hours. Long, needle shape grains were observed on the sample surface, suggesting an "abnormal" pressure-induced grain growth behavior (this has not been reported in the literature). The abnormal grain growth process was later found to be quite sensitive to the applied pressure. Results showed that the abnormal grain growth could not be observed when the applied pressure was at 5.0 kpsi or 7.5 kpsi. The upper pressure limit to induce this phenomenon still needs to be determined. Hot pressing $LaBr_3$ at 740°C for 24 hours at 10 kpsi produced a large grain microstructure (grain size ~ 20 mm x 4 mm in comparison to typical micron size grains in ceramics; see the inserted photo in Figure 19). Figure 19 gives the X-ray diffraction pattern of this hot pressed sample and shows that hot pressing has created a highly textured ceramic with a-axis (100) out-of-plane preferred orientation. These new observations, including the resulting coarser microstructure and texture development, were confirmed by additional experiments. These results suggest that highly textured ceramics can be made without introducing template seed particles. The combined

effects are highly desirable since textured ceramics can reduce refractive index mismatch at grain boundaries, and the abnormal grain growth can replace the solid-state conversion process to create a large grain microstructure. These results will improve the ceramic transparency by reducing the amount of light scattering at the grain boundary.

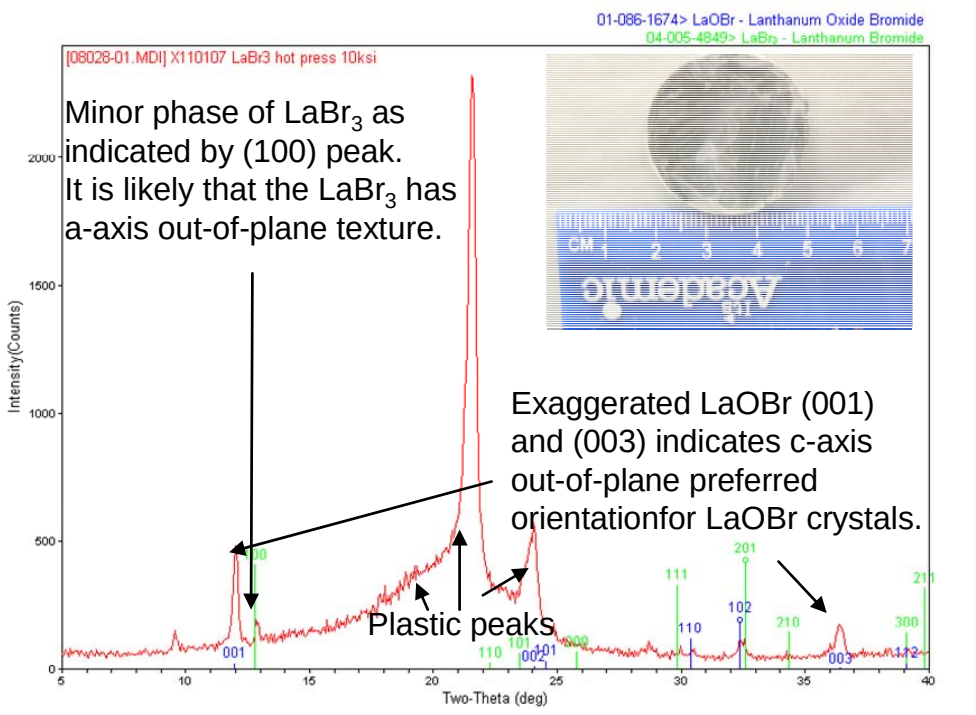

Figure 19. X-ray diffraction pattern for the hot pressed $LaBr_3$ sample (740°C, 24 hours, at 10 kpsi). Data show that a large amount LaOBr formed on the sample surface, presumably due to sample handling at the ambient conditions. The insert photo shows a pressure-induced abnormal grain growth microstructure (note the lines on the surface of sample are grain boundaries not cracks).

Figure 20. A uniaxial hot pressed partially translucent LaBr3 ceramic under a backlighting condition.

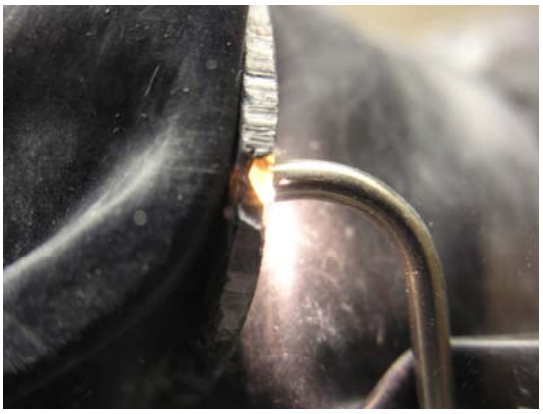

Figure 21. Light scattering at the grain boundary of a hot pressed, coarse-grained LaBr3 ceramic (thickness=3mm). Note there are two grains across the sample thickness

Two thinner samples (31.8 mm dia, 3.0 mm thick) were hot pressed, one with random powder and the other using the shear forming process, to evaluate processing effects on ceramic microstructure and translucency. Results showed that the shear forming processed sample had a coarser grain structure and a much better translucency in comparison to the random one. Figure 20 shows the sample that was processed with shear forming and uniaxial pressing at 10 kpsi at 720°C for 24 hours. The sample was illuminated with backlighting, and few areas showed that light was able to directly passing through the sample thickness. It was found that a significant amount of light was scattered at the grain boundary in these opaque areas (see Figure 21). This observation further demonstrates the importance of texture (or crystallographic alignment) to the optical quality of a birefringent polycrystalline ceramic (such as $LaBr_3$).

(2) Atmosphere-controlled hot pressing

The borrowed glovebox was cleaned and a hydraulic press was placed in the center of the glovebox for setting up an in-house designed hot press (see next section). A small diameter stainless steel tube (0.375 in. OD, or 0.25 in. ID) was installed and connected close to the hydraulic press in the glovebox for sampling the gas composition/condition during the hot pressing operation. A turbo pumped residual gas analysis (RGA) system will be connected to the glovebox after all the testing and calibration are finished.

The purity of our house Argon was measured with the RGA system equipped with a leak valve. The base pressure prior to the measurement was 1 x 10^{-8} Torr. The background gas for a typical vacuum system attached to the RGA system contains H_2O, CO and CO_2 (see details in the next paragraph). The leak valve was opened to bring the pressure at the RGA up to 8 x 10^{-6} Torr. After a couple hours with the house Argon sweeping across the leak valve, the following spectra were taken. Notice that there is no evidence of an oxygen peak (our major concern and contaminant to be removed for the Phase III development) at the mass/charge ratio of 32 in Figure 22.

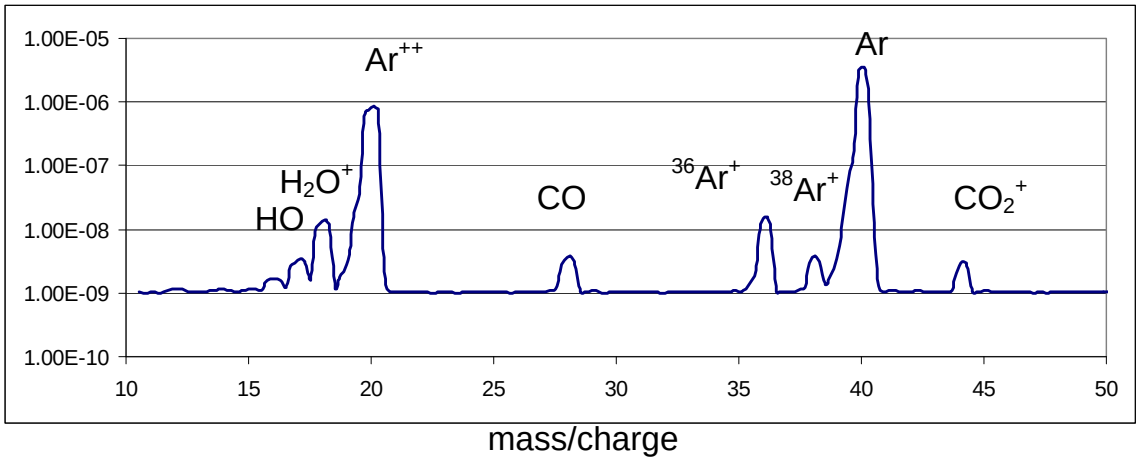

Figure 22. The residual gas analysis results for the house argon connecting through a vacuum system. Note water, carbon monoxide and carbon dioxide are coming from the vacuum system.

After the high vacuum background spectra were subtracted, it can be clearly seen that the water, carbon monoxide and carbon dioxide peaks were only from the vacuum system. All of the remaining peaks are from Argon (see Figure 23).

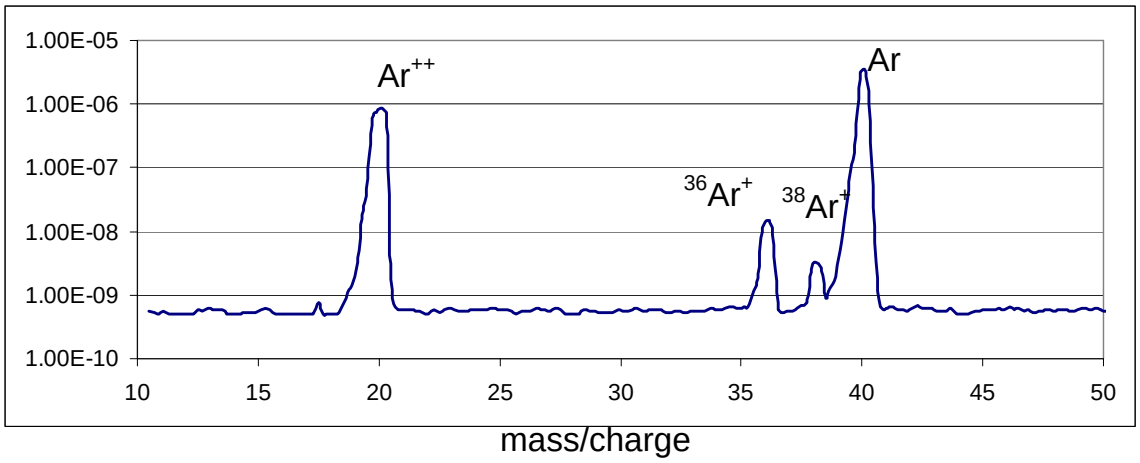

Figure 23. The residual gas analysis result for the house argon after the high vacuum background spectra was subtracted.

The mass 38 isotope of Argon has a natural abundance of 632 ppm, which further suggests that the measurement capability for this RGA system is ~100 ppm. The RGA system was used to monitor the gas condition during thermal process (for example, hot pressing) in the glovebox.

The new setup for argon-filled glovebox and hot pressing system is shown in Figure 24. In the center of the glovebox is a hydraulic press with a ceramic fiber heater (680W, Watlow) sitting on the pressing platform. The selected heater permits a maximum operation temperature (>800°C) that exceeds the melting point of lanthanum bromide (~781°C). The heater was connected to a temperature controller (Watlow) on the right. $LaBr_3$ powder prepared in the synthesis glovebox will be sealed in a can and brought into this system through the transfer port (on the right) which is equipped with vacuum and argon lines. This system will prevent moisture and oxygen contamination during the setup procedure for the graphite furnace used in the Phase I and Phase II development. Two additional thermocouples were used to monitor the temperature changes in the heater and on the top of the heater. To prevent out gassing from the refractory during heating in the glovebox, the ceramic fiber heater was baked at 800°C for 3 days. An additional 3 days bake-out was performed inside of the glovebox under a flowing argon condition to minimize gas contaminations due to the out gassing from the newly established hot press system.

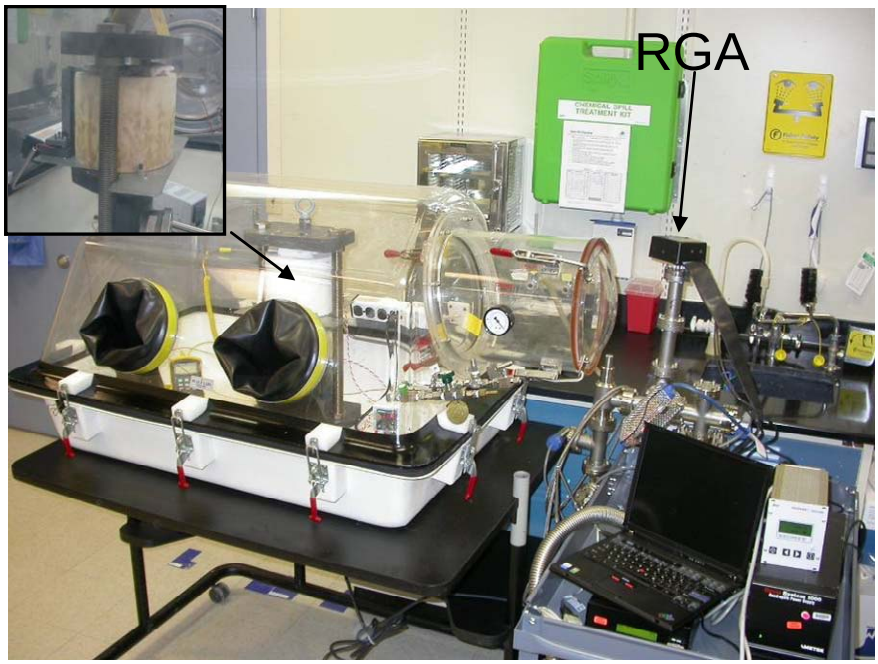

Figure 24. An in-house designed hot pressing system in a glovebox. The glovebox is connected to a turbo pumped RGA with a leak valve to monitor the gas condition during hot pressing operations.

A Sandia synthesized anhydrous powder of $La_{0.95}Ce_{0.05}Br_3$ powder, as determined by XRD, was hot pressed in the glovebox at 760°C for 48 hours at 10 kpsi in an atmosphere controlled glovebox. After hot pressing, the pellet turned black. After quartering the samples, a dark inside and round pores were observed in the sample, suggesting the processing temperature was too high as documented in an earlier report (see details in our first year's annual report)[5]. Furthermore, the sample lacked the previously observed abnormal grain growth. 20 grams of commercial powder was then hot pressed at 720°C for 2 hours and 20 minutes under the same pressure to compare the color change and porosity formation. The resulting sample is white and dense, confirming that the processing temperature was too high for the first trial run. Preliminary results showed these powders are anhydrous $LaBr_3$ with minor Cu^o contamination, presumably a result of chemical reaction between $LaBr_3$ and Cu^o (liner material) at high temperatures. However, there is no evidence of LaOBr and reduced $LaBr_3$ phases, such as LaBr, La_2Br_5, and $LaBr_2$ in the powder, as determined by XRD analysis. These results indicate we can successfully control the processing atmosphere without introducing oxyhalides in the hot pressing operation.

Some of the pulverized powder obtained from the hot pressed sample was subsequently bromine treated at 700°C and 420°C for 5 hours in a tube furnace inside of a glovebox. Bromine was introduced at room temperature by the house argon before heating up the furnace and the mixture (Br_2/Argon) was shut off after cooling down back to room temperature. Dark powder heat treated at 700°C remained black (tinted with gray), but some powder treated at 420°C turned back white and pale gray. The observation further confirmed that the loss of bromine due to the thermal stability of powder at high temperatures is the root cause for darkening behavior.

2.1.4 Task 4: Densification of ultra-fine grained $LaBr_3$ ceramics

2.1.4.1: Development approach

With many technical challenges and uncertainties during the development process, especially for the "darkening" behavior for Sandia powder, the team initiated our back up plan using the ultra-fine grain approach. A new contract with LANL (Dr. Christopher Chen at Las Alamos National Laboratory or LANL) was established under the auspices of Dr. Alan Janos form the Domestic Nuclear Detection Office, Transformational Research and Development Directorate. Two batches of powder (cerium doped $LaBr_3$) were delivered to Sandia for evaluation. One batch of powder was hot pressed at 725°C for 40 minutes at 5.7 kpsi under rough vacuum; the same condition Sandia used to produce a 3 inches diameter translucent $LaBr_3$ sample in the first year of this program.[5] The first experiment produced a white pellet with a geometric density closer to 92.5% of the theoretical value. The hot pressed sample was optically opaque under backlighting. The observation suggests that the nanosize powder produced by the melt spinner process might be more difficult to densify in comparison to a processed commercial powder.

The other approach was explored to create ultra-fine grained $LaBr_3$ ceramics, using an equal channel angular consolidation (ECAC) process at LANL. This approach is similar to the equal channel angular extrusion (ECAE)[27] process used in producing ultra-fine grained metals by severe plastic deformation. In this process, high pressure and severe deformation were imposed simultaneously to a ceramic compact sealed in a metal can (typically nickel) at high temperatures. The applied pressure at high temperature would promote densification, while the severe deformation would minimize the grain growth. The unique combination should be able to produce dense ceramics with ultra-fine microstructure. Optical quality ceramics with high light transmission can be achieved if the average diameter of the grain in the ceramic is controlled to be less the emission wavelength of the scintillator.

2.1.4.2: Development details

(1) Hot pressing of ultra-fine powder made by melt spinner process

High purity $LaBr_3$ and $CeBr_3$ powders were used as the starting materials. Pre-weighed powders were mixed in a high purity Al_2O_3 mortar and pestle. Mixed $La_{0.95}Ce_{0.05}Br_3$ powder was loaded into the BN nozzle and installed inside the induction coil. Since Both $La_{0.95}Ce_{0.05}Br_3$ powder and BN are non-conductors, a Niobium (Nb) shield was machined to serve as a coupling to the induction coil. The system was first evacuated followed by purging with Ar gas. This process was repeated again in order to ensure an oxygen and moisture free environment. The vacuum step should be beneficial in removing residual moisture if there is any. After the Ar environment is established, the induction power was turned on to heat up the mixed powders. The peak temperature was set at about 870 to 900°C with a heating rate of about 20°C/min. The copper wheel was also turn on the turning speed was increased slowly to about 2000 rpm. After the temperature is stabilized for about 2 minutes, an Ar jet with 3 psi was applied to inject the molten $La_{0.95}Ce_{0.05}Br_3$ through the nozzle opening and onto the water cooled copper wheel. The opening of the BN nozzle is about 0.019". The spun flake was sprayed into the snout section of

[27] V.V. Stolyarov, Y.T. Zhu, I.V. Alexandarov, T.C. Lowe, and Z. Z. Valiev: Grain refinement and properties of pure Ti processed by warm ECAP and cold rolling, *Mater. Sci. Eng.* **A 343** [1-2], 43 (2003).

the collecting area. To minimize the time exposed to the environment, a funnel was made as a liner for the snout. The spun nanoparticles were collected within a very short period of time to minimize the exposure time of the nanoparticle to the moisture. The melt spun $La_{0.95}Ce_{0.05}Br_3$ was then collected into a glass container purged with Ar gas. The sealed glass container was quickly transferred to a glove box.

Since the batch size is large (80 grams), a slightly higher temperature was tried to ensure a completely molten stage of the starting powders. Two melt spinning runs were performed. The first run with 80 grams was heated to about 900°C and the resulting flakes seem to be rather thick compared to the previous runs. It is believed that 900°C is too high to melt the starting powders. The high temperature caused the molten $La_{0.95}Ce_{0.05}Br_3$ to have a low viscosity and a faster stream to the copper wheel. The second run with 80 grams was controlled at about 870°C and the viscosity of the molten $La_{0.95}Ce_{0.05}Br_3$ seems to be more controllable. The flake was much thinner and the result was more consistent with previous runs. Both runs with more than 50 grams each were delivered to SNL for hot pressing. One batch of powder was hot pressed at 725°C for 40 minutes under a rough vacuum; the same condition Sandia used to produce a 3 inches diameter translucent $LaBr_3$ sample last year.[5] The first experiment produced a white pellet with a geometric density closer to 92.5% of its theoretical value. The hot pressed sample is optically opaque under backlighting and with few dark spots on the surface (presumably due to the reduced La_2Br_3). This observation is consistent with previous results obtained at LANL last year, which immediately suggests that the densification behavior of this melt spinning powder is quite different from these powders prepared by the ball milled commercial material. In addition, the white color of this hot pressed pellet suggests that a short processing time at high temperature could minimize the loss of bromine and reduce the color centers. The second batch of powder was hot pressed at 760°C for 40 minutes at 5.0 kpsi under vacuum. The sample was molten and squeezed out from the alumina die during hot pressing; presumably due to the processing temperature too close to its melting point (according to the phase diagram study in this report where the melting point for this composition is at 761 °C).

(2) Equal channel angular consolidation of $LaBr_3$ ceramics

Six nickel (Ni) containers were machined from a Ni tube with 10 mm OD and 8 mm ID. Twelve end caps were machined from a nickel rod to fit the Ni containers. Figure 25 shows the typical machined Ni tube and end caps. One of the end caps was first welded to the Ni tube to seal one end. Three different powders were selected for the ECAC experiments including (1) hand mixed raw powder, (2) melt spun at 900°C, and melt spun at 870°C. Each powder was loaded into two containers inside a glove box with a total of six containers. After powders were loaded, the other end cap was inserted into the container inside the glove box to seal the container. All six containers with powder loaded were sealed by vacuum electron beam welding. All six samples have been consolidated using the ECAC. To increase the size of the samples, all were enclosed in a thinner nickel can with about 1.5 mm thick wall. Sample #1 was ECACed at 720 °C. The first sample had cracking after the ECAC process at 30,000 psi, which might be caused by the thinner wall. Sample #2 was ECACed at a reduced back pressure of 15,000 psi. To investigate the effect of multiple passes, only one pass was performed on sample #2. Sample #2 was cut inside a glovebox using a slow saw with a silicon carbide (SiC) blade, perpendicular to the long axis of the Ni tube to obtain several ring samples. The as-cut ring shows a translucent

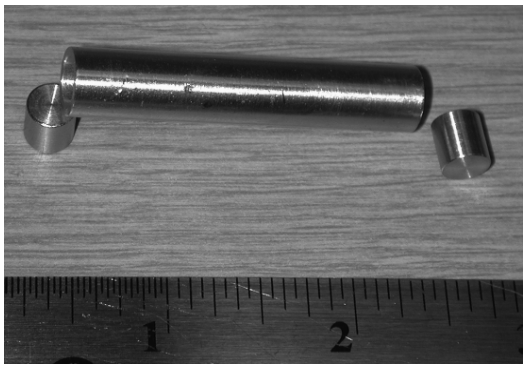

Figure 25. The typical machined nickel (Ni) tube and end caps for ECAC Process.

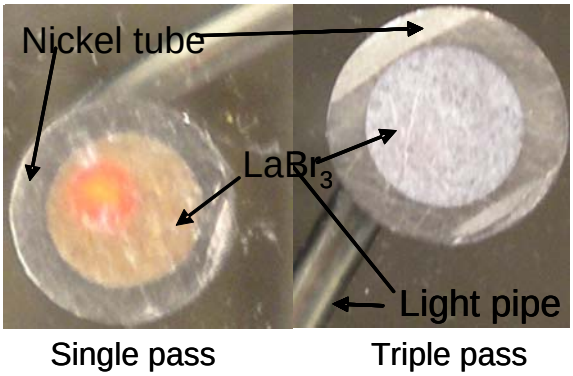

Figure 26. A comparison of translucency under a backlighting condition between samples prepared by the ECAC process with a single and triple pass

appearance, which is an indication of high sintered density. More polishing work is underway to show the microstructure and the transparency of the sintered rings.
Sample #3 was ECAC'ed at 720 °C with two passes. A third pass will be performed to complete the random orientation. As soon as the third pass is completed, sample #3 will be cut inside the glovebox and polished to compare with sample #2, which had single pass. Based on the results from the single pass and 3 passes, more samples will be ECACed to optimize the starting melt spinning powders.

Two sliced samples (2 mm thick) made from ECAC process (15 kpsi, 720°C) were polished to examine their translucency. These samples were cut perpendicular to the long axis of the Ni tube to obtain several ring samples (the nickel ring was from the cross-cut of a cylindrical metal can with densified $La_{0.95}Ce_{0.05}Br_3$ inside after ECAC process). These samples were polished down to 0.3 µm in a glove box. Figure 26 shows these samples under a backlighting condition. Results indicated that the sample with a single pass (#5) through the equal channel was more translucent (can easily see the backlighting through the sample thickness) than the triple-passed sample (#3), presumably due to a finer grain structure. The particle size determined by X-ray diffraction (see Figure 27) showed that the crystallite size for the single pass material was about 100 nm which is roughly the upper limit of our detection for size measurements. In addition, the grains in the sample exhibit a random oriented diffraction pattern, indicating the shearing action during consolidation did not introduce texture for nanocrystalline size powder.

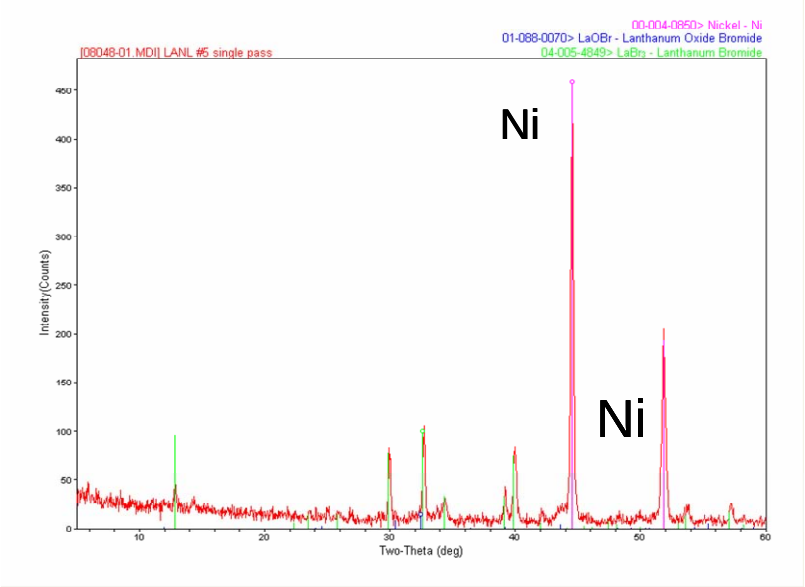

Figure 27. X-ray diffraction pattern of a single pass ECAC sample. Pattern shows peak broadening suggesting an ultrafine grained microstructure. Ni peaks come from metal can used in ECAC process.

One more melt spinner run was performed to get more nanoparticle $LaBr_3$:Ce for ECAC. The melt spun run seems to be unstable, which results in less than perfect nanoparticles. The melt spun powder (#8) was loaded into another nickel can, which was then vacuum e-beam welded. ECAS was performed on this can at 720 °C with single pass. The sample #8 after cutting showed fully dense structure but not as translucent as sample #5. It is believed that the starting powder is extremely critical in getting a transparent polycrystalline $LaBr_3$:Ce together with an optimized consolidation condition (e.g. lower temperature). These activities came to a halt as funding depleted in December 07.

3. DIFFICULTIES ENCOUNTERED AND RECOVERY ACTIONS

The project team successfully met the majority of the goals set for Phase II and Phase III, as described above. However, we encountered several problems during the development process. Some of these difficulties were overcome; others have yet to be resolved. Table 4 lists the difficulties encountered in this project and the recovery actions taken or recommended. Issues are discussed in greater detail in the section below.

Table 4. Difficulties Encountered and Recovery Actions

Issues		Response	T/B/S	Impact
1.	*Purchasing glassware, chemical, equipment for processing*	*Glassware/equipment ordered to meet urgent needs for reducing metal contamination and enhancing deposition rate for seed crystal synthesis (issue 5). A glass fluidized reactor was designed and fabricated to enhance dehydration efficiency (issue 7).*	*S*	*None*
2.	*Thermal and hydrogen release for large batch processing development*	*The hydrogen byproduct will work in glove box and help to keep the system clean.*	*T*	*None: Completed November 2007.*
3.	*Control morphological properties of seed particle – during dehydration*	*Both seeding and freeze drying did not yield desirable results. Development activity switched to the vapor phase synthesis method (issue 5).*	*T*	*New approach (5) has been identified. Could delay result. (Completed: April, 07)*
4.	*Seed particle characterization – at high temperature large seed crystal turned in nanocrystalline aggregates*	*Thermal analysis data and TEM results prompted to develop and evaluate new approaches including controlled recrystallization from direct acidification process (issue 3) and vapor phase deposition (issue 5).*	*T*	*Initiate new approaches to resolve this issue. Could delay results.(Completed: March, 07)*
5.	*Vapor phase transport approach for seed crystals preparation – a steep learning curve*	*The process conditions that control the morphology of these particles are unknown and will probably be strongly dependant on processing conditions. Different gas composition (e.g. introduce bromine gas) will be explored to assist $LaBr_3$ formation. Modified a new alumina reactor to enhance efficiency and to minimize silicon contamination.*	*T,S*	*Could delay results; reactor design and material selection seem to be crucial for the success.*

6.	*Training new technologist – enhance overall productivity*	*Hands-on synthesis process, powder characterization and processing were completed. Technologist has become familiarized with all the characterization tools.*	*S*	*None Complete: November 2007*
7	*Identify contamination or source of darkening behavior – first residual water, later residual oxygen*	*Darkening was contributed to the partial reduction of $LaBr_3$ due to the presence of trace amounts of water. New evidence has shown oxygen could be the culprit. Additional experiments are underway to determine the root cause.*	*T,S*	*Delay in development, affect performance.*
8	*Evaporation route for seed particles – seeds growth from MeOH showed a reconstructive phase change*	*Needle shape seed particles were isolated. However, these seeds have a similar issue as previous seeds grown from THF and are not suitable for texture development. Since then, all efforts have focused on the vapor phase transport process (issue 5) for seed preparation.*	*T,S*	*Complete: September 2007. Focus on vapor phase synthesis*
9	*Pressure-induced abnormal grain growth and texture development- a new approach for texture development (seedless)*	*Initial observation was experimentally re-confirmed. However, sample was not completely transparent. The incorporation of seed crystals will be explored to enhance optical quality of $LaBr_3$ ceramics.*	*T,S*	*If successful, it will be the best approach to produce optical quality sample.*
10	*Equal channel angular sintering – reduce grain structure to enhance optical transparency*	*Samples after a single extrusion process look promising. Need to optimize the process with a lower consolidation temperature.*	*S*	
11	*Verify residual water by NMR study*	*Results from NMR studies of label ^{17}O and solid state ^{139}La indicate that our vacuum evaporation is effective to remove residual water for initial lanthanum bromide hydrates.*	New	Task terminated
12	*Control oxygen contamination*	*Powders prepared under different conditions were sealed in quartz tubes and fired at 700°C, to verify the oxybromide formation. A new Schlenk system for bromine treatment has been designed and sent to fabrication.*	On schedule	Task terminated
13	*Control processing/ handling condition*	*The RGA has been connected to the glovebox for monitoring the processing environment during hot pressing. The system now works properly with a detection limit at ~ 100 ppm.*	*T*	*This task is on schedule. It will help to monitor and control processing environment.*
14	*Thermal process for densification*	*It appears that the darkening is introduced by prolong, high temperature densification process. Additional experiment is underway to verify this observation.*	*T*	*New approaches need to be developed in order to address this issue.*

Impact type: T/B/S means **T**echnical, **B**udget and/or **S**chedule;
Severity Color Code: R=Project likely at risk, Y= Milestones/Deliverables likely at risk, G=Milestones/Deliverables slightly at risk, B=Issue resolved.

3.1 Technical Risks

Issue 1: There were many occasions where additional chemicals, new glassware and extra ES&H issues needed to address in the different stages of development. These activities sometimes impacted the overall program schedule. For example, it took almost two months to get our first liquid bromine and more than one month to get our quartz reactor when metal contaminations during seed crystal growth was first identified.
Issue 2: Hydrogen released from the direction acidification process will help the re-generation process for the catalyst in the glove box.

Issue 3: Attempts to control seed crystal morphology directly from the dehydration process by seeding and freezing drying did not yield desirable results. When the liquid nitrogen was first introduce into the direct acidification solution, crystalline lanthanum bromide hydrates formed before water became frozen. During the drying process, these hydrates underwent a series of reconstructive phase transformations and lost the distinct morphology; therefore, these particles could no longer serve as templates for the texture development.

Issue 4: Although the highly anisotropic seed crystals synthesized from THF can be easily aligned by a shear forming process, TEM results showed after a thermal process (used in the densification and texture development processes) the large crystals turned into nanocrystalline aggregates and lost their function as templates for the texture development. Searching for new approach, we found that platelet $LaBr_3$ crystals can be grown from a vapor phase transport process. Therefore, the task to grow seed crystals from a hot THF solution was terminated.

Issue 5: We have experienced several challenges during the development phase for vapor phase seed crystal growth. Most of these issues are associated with the chemical reactions between bromine gas and reactor at high temperatures. Initially we found iron and chromium contaminations which can be attributed to a corrosive reaction between bromine gas and stainless steel flanges at each end of the reactor. After changing to a quartz tube under a flow argon condition, seed crystals were deposited in an undesirable location, suggesting vapor phase transport in the reactor need to be optimized. Lastly, when a closed quartz system was used, a significant amount of silicon contamination was discovered, indicating a chemical reaction occurred between quartz tube and bromine gas under a static condition. To overcome these challenges, we need to optimize the reactor design to enhance the production efficiency and to use an alumina tube to minimize chemical contamination.

Issue 6: A new technologist was hired at the beginning of the second phase. She has been trained on chemical synthesis, the use of Schlnek line and glove box operation, pressure safety and cryogenic trainings, handling sensitive materials, furnace and reactor set-up and operations, powder processing, and XRD and SEM sample preparation. She won the best poster award for her work on "The dehydration behavior of lanthanum bromide hydrates" in the graduate category in the 19th Rio Grande Advanced Materials Symposium at Albuquerque, NM, October 10, 2007.

Issue 7: This issue has been the major focus during this year. We have systematically ruled out the organic solvents during synthesis and the loss of bromine during dehydration as the culprit for the darkening of hot pressed samples. Later on we sought the answers from residual water in the powder and oxygen from processing environment. It was found that a rigorous process control is the key to eliminate oxybromide formation. In the next phase we will use oxygen getters and constantly monitor the processing condition to assure the reproducibility.

Issue 8: The growth of anhydrous $LaBr_3$ seed crystals from a MeOH solution was initiated at August 2007. After an extensive study, it was found that these needle shape crystals experienced several decomposition steps and produced nanocrystalline clusters similar to the dehydration of lanthanum bromide hydrates. Therefore, the approach is not suitable for the preparation of template seeds. However, this approach, when handled carefully, produced anhydrous $LaBr_3$ after a high temperature treatment (> 500 °C); therefore, we will continue to pursue this approach to produce phase pure, anhydrous $LaBr_3$ powder.

Issue 9: After the second program review, we decided to re-focus on densification process since it is the key to achieve optical quality ceramics. An Inconel 718 super alloy die was made to enhance densification process by doubling the applied pressure during hot pressing. The results were quite encouraging. It was found that external pressure during densification can effectively induce texture in $LaBr_3$ ceramics. Furthermore, above a critical pressure (> 7.5 ksi), an abnormal grain grown were observed. The combined effects are highly desirable since textured ceramics can reduce refractive index mismatch at grain boundaries, and the abnormal grain grown can reduce the amount of grain boundary area. Therefore, the overall effect will significantly reduce the amount of light scattering at the grain boundary. Further improvement of the optical quality can be achieved by creating a highly textured ceramic green body (introducing seed crystals in the forming process) before final densification.

Issue 10: Using an ultrafine grained approach to achieve optical quality ceramics was a backup plan and was initiated at the beginning of the second phase. The LANL approach was selected based on the technical merits. After we received the final approval from DHS headquarter in August, the program has made great strides in powder processing and densification using a melt spinner and equal channel angular consolidation (ECAC), respectively. It was noticed immediately that nano-size powder made by melt spinner process is harder to densified in comparison to Sandia or commercial powder. However, after hot pressing for 40 minutes at 725°C powder remains white with few dark spots suggesting LANL powder has less residual water or second phase (such as LaBrO). Samples fabricated by ECAC were uniform and partially translucent. Results show the translucency highly depended on processing condition (such as, processing temperature or sample was consolidated by a single-pass or a triple-pass). However, due to the time constraint the process has not been optimized. Increasing sample size in the future will need a significant capital investment on tooling (estimated ~ $120K).

Issue 11: Using NMR, we have confirmed that the vacuum dehydration is effective to remove bounded water from hydrate precursors. Therefore, darkening is not a direct result of residual water and oxyhalide formation.

Issue 12: Melting experiment, using sealed quartz ampoules, demonstrated the importance of powder handling and suggested darkening might come from the intrinsic thermal instability of the $LaBr_3$, particularly at the surface layer of the melt.

Issue 13: An in-house built hot pressing system was used in the argon filled glovebox to eliminate the exposure of air (oxygen) or moisture during powder handling and hot pressing. Additional bake up was performed to eliminate the out gassing from the heating unit. Hot pressing after the additional bake out procedure produced high density, oxyhalide free specimens. However, hot pressed pellets were still dark. The technical issues associated with the darkening behavior seem to be quite challenging. Bromine treatment at lower temperature (420°C) later confirmed that darkening might due to the loss of bromine during a prolonged high temperature hot pressing operation.

Issue 14: Both the melting experiment (in sealed glass ampoules) and hot pressing experiments indicate that the darkening issue of hot pressed sample might be attributed to the intrinsic instability of $LaBr_3$ at high temperature, where $LaBr_3$ starts to loss bromine in the structure and produces color centers in the material. If this is true, this is particular difficult for fine grained, chemically synthesized powder. A lower temperature (< 450°C), longer pressing time will be explored to see if one can achieve high density without introducing darkening into the hot pressed samples. If the approach can not achieve high density, this issue will be the ultimate challenge for densification of ultra-fine grained ceramic powder.

3.2 Budget Risks

There were no significant budget issues during Phase II and Phase III programs.

3.3 Schedule Risks

Because the development of new processing routes for seed particle preparation (Issues 3, 4, 5, and 8) is highly empirical, it is difficult to control progress. Nonetheless, the concepts and approaches developed are based on educated, engineering judgments. Time constraints and reactor design had shown to be a risk factor for schedule.
Characterization of densification and selective grain growth and texture development in the ceramic matrix (Issue 9) requires significant resources and time. Our ability to conduct experiments sometimes depends on the availability of the furnace and hot press. Therefore, even with a well planned experiment schedule, some scheduling conflicts can not be completely ruled out.

4. LESSONS LEARNED AND THEIR IMPACT ON FUTURE R&D

We have nothing to report on lessons learned at this time.

5. ANY ADDITIONAL INFORMATION REQUIRED

No report of additional information is needed at this time.

6. HONORS, AWARDS, TECHNICAL PRESENTATIONS AND PUBLICATIONS'

6.1 Honors and Awards

M. R. Sanchez, P. Yang, C. B. DiAntonio, T.J. Boyle, L. A. Ottley, and M. A. Rodriguez, "Vacuum Dehydration of Lanthanide Bromide Hydrates," The 19th Annual Rio Grande Advanced Materials Symposium, Albuquerque, New Mexico, October 9, 2007. - Poster Award - 1st Place (Graduate Level)

L. A. M. Ottley, T. J. Boyle, R. M. Sewell, C. M. Baros, P. Yang, and M. A. Rodriguez, "Lanthanum Halide Solvated Compounds", The 19th Annual Rio Grande Advanced Materials Symposium, Albuquerque, New Mexico, October 9, 2007. - Poster Award – 2nd Place (Graduate Level).

6.2 Technical Presentations

P. Yang, C. B. DiAntonio, T. J. Boyle, M. A. Rodriguez, and M. R. Sanchez, "Dehydration and Solid Solution Formation for the $LaBr_3$-$CeBr_3$ Binary System," SPIE Optics + Photonics 07, Penetration Radiation Systems and Applications VIII, San Diego, CA, (2007).

T. J. Boyle, P. Yang, and M. A. Rodriguez, "Synthesis of Lanthanum Halides," SPIE Optics + Photonics 07, Penetration Radiation Systems and Applications VIII, San Diego, CA, (2007).

M. R. Sanchez, P. Yang, C. B. DiAntonio, T.J. Boyle, L. A. Ottley, and M. A. Rodriguez, "Vacuum Dehydration of Lanthanide Bromide Hydrates," The 19th Annual Rio Grande Advanced Materials Symposium, Albuquerque, New Mexico, October 9, 2007.

L. A. M. Ottley, T. J. Boyle, R. M. Sewell, C. M. Baros, P. Yang, and M. A. Rodriguez, "Lanthanum Halide Solvated Compounds", The 19th Annual Rio Grande Advanced Materials Symposium, Albuquerque, New Mexico, October 9, 2007.

T. J. Boyle, P. Yang, L. A. M. Ottley, S. Hoppe, M. Rodriguez, T. M. Alam, "Fabrication and Characterization of ceramic Lanthanide Halides Materials for Scintillator Applications," Rare Earth Conference, Tuscaloosa, AL, June 22-26, 2008.

6.3 Publications

P. Yang, C. B. DiAntonio, T. J. Boyle, M. A. Rodriguez, and M. R. Sanchez, "Dehydration and Solid Solution Formation for the $LaBr_3$-$CeBr_3$ Binary System." SPIE Opcitcs + Photonics 07, Penetration Radiation Systems and Applications VIII Conference Proceedings 670709, San Diego, CA, (2007).

M. A. Rodriguez, D. Harris, T. J. Boyle and P. Yang, "A Beryllium Dome Specimen Holder for XRD Analysis of Air Sensitive Materials," Powder Diffraction, **23** [2], 121-4, (2008).

T. J. Boyle, L. A. M. Ottley, P. Yang, T. M Alam, M. A. Rodriguez, "Methanolation of Lanthanum Bromide Hydrate," Submitted to *Inorganic Chemistry* (2008).

T. J. Boyle, L. A. M. Ottley, M. A. Rodriguez, T. M. Alam, P. Yang, R. M. Sewell, C. M. Baros, S. K. McIntyre, and M. R. Sanchez," Facile Synthesis of Structurally Characterized lanthanide/Group 3 Halide Hydrates, Anhydrous Halides, and Solid-Solution of Mixed lanthanide Halide Materials," Submitted to *Inorganic Chemistry*, (2008).

P. Yang, Timothy J. Boyle, Mark A. Rodriguez, Todd M. Alam, Christopher B. DiAntonio, Margaret R. Sanchez, and Leigh Anna M. Ottley, "Vacuum Dehydration and Solid Solution Formation of $LaBr_3$-$CeBr_3$," In preparation to be submitted to J. of Amer. Ceram. Soc., (2008).

7. OVERALL MANAGEMENT

7.1 Account of Funds Expended by Program, Project, and Tasks

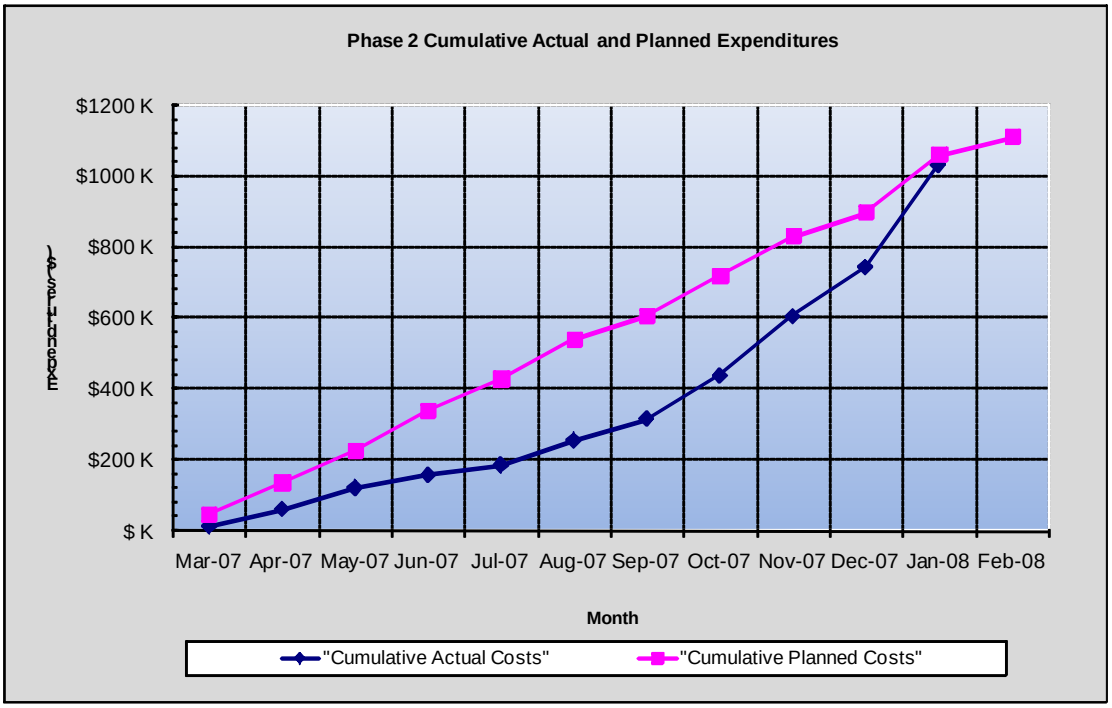

Figure 28. A comparison of expended funds with projections from contract start (Phase II, FY07).

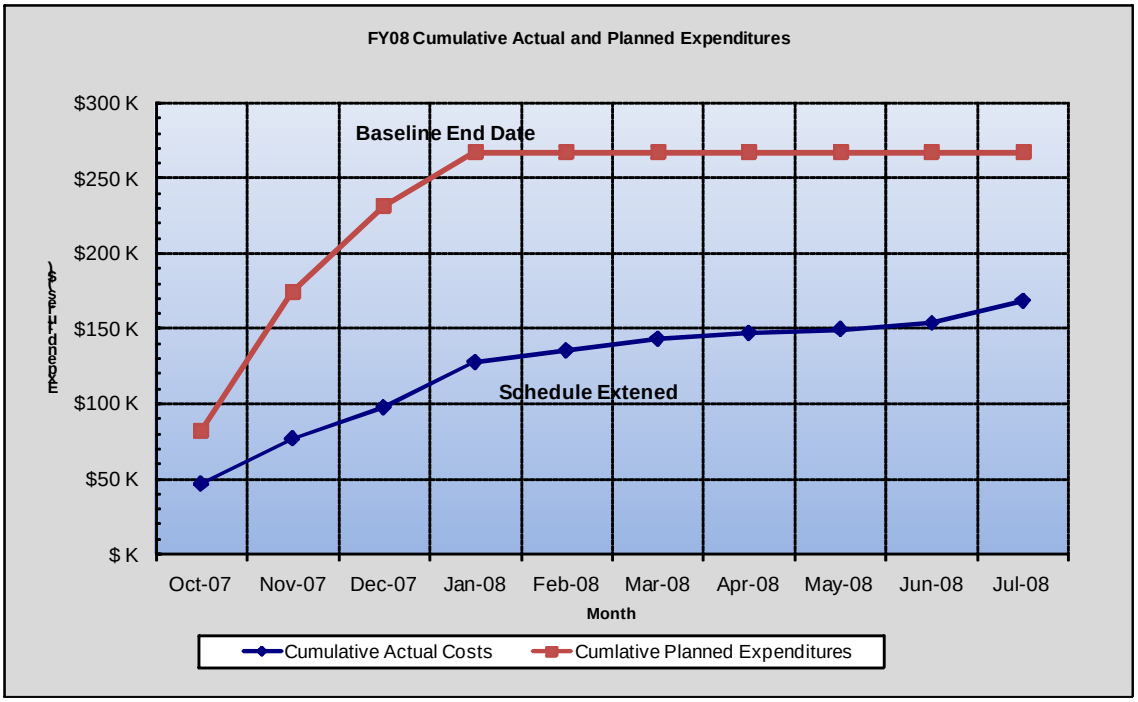

Figure 29. A comparison of expended funds with projections from contact start (Phase III, FY08).

7.2 FY07 Gantt Chart

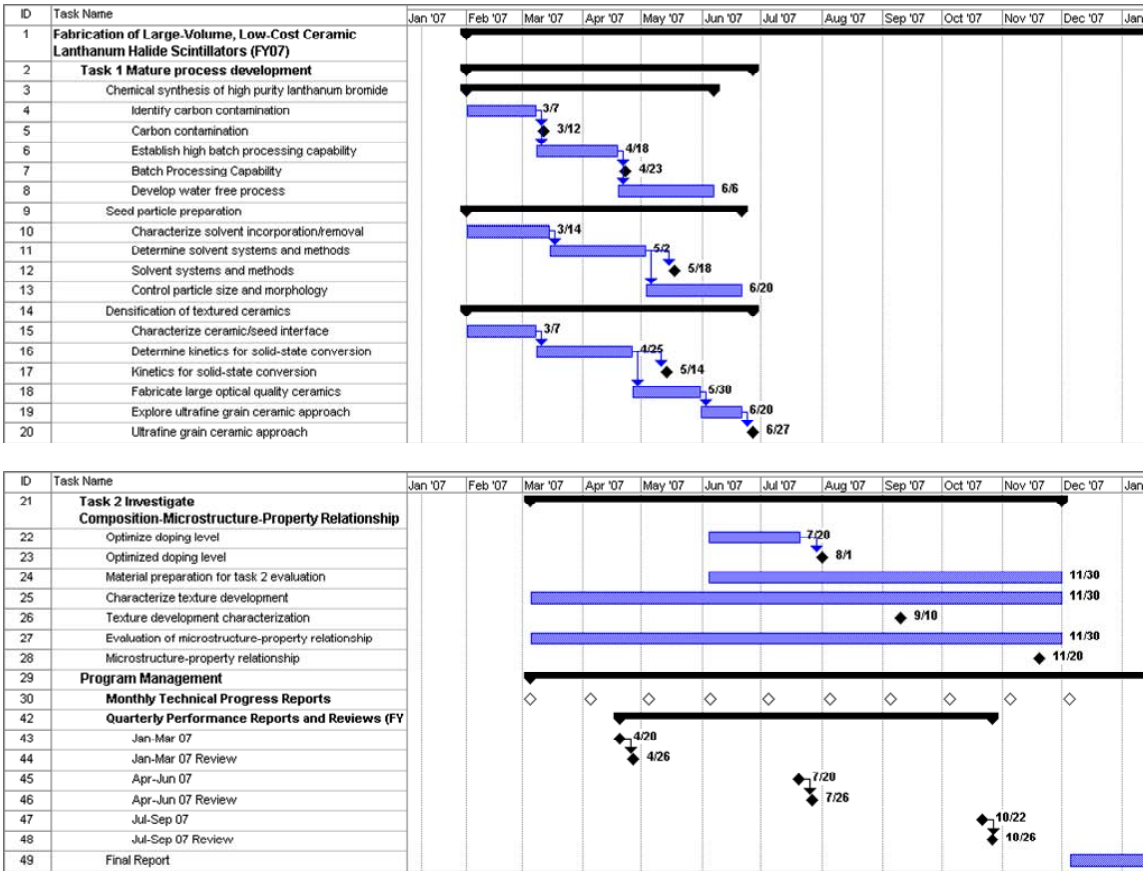

Figure 30. A Gantt chart for FY07 project plan and schedule.

7.3 FY08 Gantt Chart

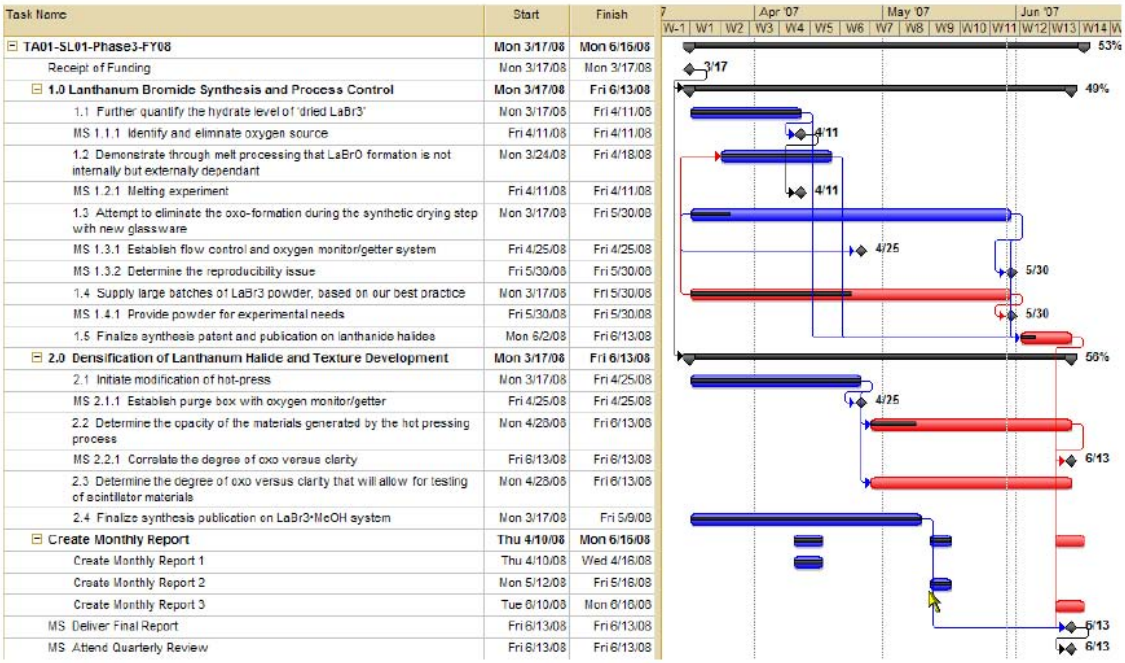

Task Name	Start	Finish
TA01-SL01-Phase3-FY08	Mon 3/17/08	Mon 6/16/08
Receipt of Funding	Mon 3/17/08	Mon 3/17/08
1.0 Lanthanum Bromide Synthesis and Process Control	Mon 3/17/08	Fri 6/13/08
1.1 Further quantify the hydrate level of 'dried LaBr3'	Mon 3/17/08	Fri 4/11/08
MS 1.1.1 Identify and elimnate oxygen source	Fri 4/11/08	Fri 4/11/08
1.2 Demonstrate through melt processing that LaBrO formation is not internally but externally dependant	Mon 3/24/08	Fri 4/18/08
MS 1.2.1 Melting experiment	Fri 4/11/08	Fri 4/11/08
1.3 Attempt to eliminate the oxo-formation during the synthetic drying step with new glassware	Mon 3/17/08	Fri 5/30/08
MS 1.3.1 Establish flow control and oxygen monitor/getter system	Fri 4/25/08	Fri 4/25/08
MS 1.3.2 Determine the reproducibility issue	Fri 5/30/08	Fri 5/30/08
1.4 Supply large batches of LaBr3 powder, based on our best practice	Mon 3/17/08	Fri 5/30/08
MS 1.4.1 Provide powder for experimental needs	Fri 5/30/08	Fri 5/30/08
1.5 Finalize synthesis patent and publication on lanthanide halides	Mon 6/2/08	Fri 6/13/08
2.0 Densification of Lanthanum Halide and Texture Development	Mon 3/17/08	Fri 6/13/08
2.1 Initiate modification of hot-press	Mon 3/17/08	Fri 4/25/08
MS 2.1.1 Establish purge box with oxygen monitor/getter	Fri 4/25/08	Fri 4/25/08
2.2 Determine the opacity of the materials generated by the hot pressing process	Mon 4/28/08	Fri 6/13/08
MS 2.2.1 Correlate the degree of oxo verses clarity	Fri 6/13/08	Fri 6/13/08
2.3 Determine the degree of oxo versus clarity that will allow for testing of scintillator materials	Mon 4/28/08	Fri 6/13/08
2.4 Finalize synthesis publication on LaBr3•MeOH system	Mon 3/17/08	Fri 5/9/08
Create Monthly Report	Thu 4/10/08	Mon 6/16/08
Create Monthly Report 1	Thu 4/10/08	Wed 4/16/08
Create Monthly Report 2	Mon 5/12/08	Fri 5/16/08
Create Monthly Report 3	Tue 6/10/08	Mon 6/16/08
MS Deliver Final Report	Fri 6/13/08	Fri 6/13/08
MS Attend Quarterly Review	Fri 6/13/08	Fri 6/13/08

Figure 31. A Gantt chart for FY08 project activities, milestones, and schedule.

DISTRIBUTION

3	MS1245	Pin Yang, 02454
1	MS1349	Timothy J. Boyle, 01815
1	MS1411	Nelson S. Bell, 01816
1	MS1349	Robin M. Sewell, 01815
1	MS1411	Mark A. Rodriguez, 01822
1	MS1245	Margaret R. Sanchez 02454
1	MS1349	William F. Hammetter, 01815
1	MS1411	James A. Voigt, 01816
1	MS9004	William P. Ballard, 08100
1	MS0899	Technical Library, 09536

2 Department of Homeland Security
Domestic Nuclear Detection Office
Attn: Alan Janos
Anacostia Naval Annex, Bldg 410
245 Murray Lane, SW
Washington DC 20528